Petrological and Geochemical Characteristics of Egyptian Banded Iron Formations: Review and New Data from Wadi Kareim

K. I. Khalil[1], and A. K. El-Shazly[2]*

[1] Geology Department, Faculty of Science, University of Alexandria, Moharram Bey, Alexandria, Egypt
[2] Geology Department, Marshall University, 1 John Marshall Dr., Huntington, WV 25755

*Corresponding Author (e-mail: elshazly@marshall.edu).

# of words in text: 8307
# of words in references: 2144

Abbreviated title: Egyptian BIFs

Abstract

The banded iron formations in the eastern desert of Egypt are small, deformed, bodies intercalated with metamorphosed Neoproterozoic volcaniclastic rocks. Although the 13 banded iron deposits have their own mineralogical, chemical, and textural characteristics, they have many similarities, the most notable of which are the lack of sulfide and paucity of carbonate facies minerals, a higher abundance of magnetite over hematite in the oxide facies, and a well-developed banding/ lamination. Compared to Algoma, Superior, and Rapitan type banded iron ores, the Egyptian deposits have very high Fe/Si ratios, high Al_2O_3 content, and HREE-enriched patterns. The absence of wave-generated structures in most of the Egyptian deposits indicates sub-aqueous precipitation below wave base, whereas their intercalation with poorly sorted volcaniclastic rocks with angular clasts suggests a depositional environment proximal to epiclastic influx. The Egyptian deposits likely formed in small fore-arc and back-arc basins through the precipitation of Fe silicate gels under slightly euxinic conditions. Iron and silica were supplied through submarine hydrothermal vents, whereas the low oxidation states were likely maintained in these basins through inhibition of growth of photosynthetic organisms. Diagenetic changes formed magnetite, quartz and other silicates from the precipitated gels. During the Pan-African orogeny, the ore bodies were deformed, metamorphosed, and accreted to the African continent. Localized hydrothermal activity increased Fe/Si ratios.

Keywords: banded iron formations, Central Desert of Egypt, Neoproterozoic, island arcs, magnetite, hematite

Banded iron formations (BIFs) are typically low grade (>15% Fe, usually 25–35% Fe), high tonnage deposits reaching hundreds of meters in thickness and up to thousands of kilometers in lateral extent (James 1954). They typically consist of layers rich in iron oxides alternating with layers rich in silica/silicates, and appear to be almost restricted to Archean and Palaeoproterozoic terranes (Klein & Beukes 1993a; Abbott & Isley 2001; Huston & Logan 2004). Banded iron formations are widely accepted as products of chemical precipitation of Fe^{2+} and Fe^{3+} oxides and hydroxides, Fe-rich silicates, and silica in a marine environment, followed by significant diagenetic and metamorphic modification (e.g. Trendall & Blockley 1970; Ayres 1972; James 1992; Klein & Beukes 1993a; Mücke *et al.* 1996). Because present-day oxygen levels in oceans prevent Fe^{2+} from remaining in solution and cause it to rapidly precipitate as Fe^{3+} compounds, the paucity of BIFs in Neoproterozoic and Phanerozoic rocks has been linked to the Great Oxygenation Event (GOE) at *c.* 2.4 Ga (e.g. Garrels *et al.* 1973; Simonson 2003; Klein 2005).

Based on geological setting and inferred mode of formation, Gross (1965 & 1980) classified BIFs into two main types, 1) a submarine volcano-sedimentary Algoma type, typically of Archaean age, and 2) a shallow marine Superior type deposit with some continental source material, typically of Palaeoproterozoic age. Younger deposits, like the Neoproterozoic Rapitan type (e.g. Klein & Beukes 1993b; Klein & Ladeira 2004), are also recognized as BIFs, but are far less abundant compared to the Archean – Early Proterozoic deposits (e.g. Klein 2005). In addition to geological setting and inferred mode of formation, mineralogy, texture, and chemistry are often used for the further classification of BIF. For example, Webb *et al.* (2003) in their study of the Superior type BIFs at Hamersley Province, Western Australia, identified a “fresh” deposit predominated by magnetite, siderite and quartz, and characterized by Fe/Si *c.* 1.8, and an “altered” deposit dominated by hematite, quartz and goethite, with Fe/Si > 2.

In Egypt, BIFs occur in 13 localities in an area of *c*. 30,000 km^2 in the Central Eastern Desert (Fig. 1). Those BIFs contain estimated total reserves of *c*. 53 Mt of Fe, which have yet to be exploited (Dardir 1990). Although most of those BIFs have been classified as Algoma type (e.g. Sims & James 1991), they have many features that distinguish them from that type of BIF. The most notable difference is that they are intercalated with Neoproterozoic volcaniclastic sediments of intermediate composition rather than the typical Archean/Palaeoproterozoic basic volcanic rocks associated with most Algoma type BIFs (e.g. Gross 1996; Klein 2005; Bekker *et al.* 2010). Another striking feature is their relatively high Fe/Si ratios of 1.8–6.2 (as opposed to an average ratio of 1.2 for Algoma type deposits; Gross & McLeod 1980; Klein & Beukes 1992), making them potentially attractive mining

targets, and allowing for their subdivision into altered ores (Fe/Si >3.0; e.g. Gebel Semna, Hadrabia, Um Shadad, and Wadi Kareim) and relatively "fresh" ores (Fe/Si <3; e.g. Wadi El Dabbah, and Um Nar; Fig. 2). Although most Egyptian BIFs have been studied in recent years (e.g. El Habaak & Mahmoud 1994; Salem *et al.* 1994; Bekir & Niazy 1997; Essawy *et al.* 1997; El Habaak & Soliman 1999; Takla *et al.* 1999; Khalil 2001 & 2008; Salem & El-Shibiny 2002; Noweir *et al.* 2004), their origin and evolution are still debated. Some authors suggest a sedimentary model for Egyptian BIF formation on a continental shelf (e.g. El Aref *et al.* 1993; El Habaak & Soliman 1999). Other authors favor a model relating the Egyptian BIFs to submarine volcanism and hydrothermal activity in an island arc setting (Sims & James 1984; El Gaby *et al.* 1988; Takla *et al.* 1999; El Habaak 2005). In contrast, Salem *et al.* (1994) proposed a contact metamorphic origin for magnetite ore in El Emra (#10, Fig. 1).

In this paper, we present a review of the field relations, petrology, and geochemistry of the Egyptian BIFs, with special emphasis on two of them, namely Wadi Kareim and Wadi El Dabbah (#5 and #6, Fig. 1). Despite their close proximity to each other, Wadi Kareim is an "altered" BIF whereas Wadi El Dabbah is a "fresh" deposit. Data on petrography, mineral chemistry, and whole-rock chemical compositions of these two deposits are either new (Wadi Kareim) or have been published locally in conference proceedings (Wadi El Dabbah and Gebel Semna) (Khalil 2001 & 2008). The main goal of this review is to focus on the unique geochemical and geological features of the Egyptian BIFs, and to shed some light on the various proposed models about their origin and evolution in the context of the tectonic setting and evolution of the Precambrian shield of Egypt.

GEOLOGICAL SETTING AND FIELD RELATIONS

General Setting

The Egyptian BIFs are interbedded with Precambrian basement units that crop out in the central part of the Eastern Desert (Fig. 1). These units, which amalgamated during the Neoproterozoic Pan-African Orogeny, record a history of six tectonic stages (Fig. 1; Table 1; cf. El-Gaby *et al.* 1990; Kroner & Stern 2004; Stern *et al.* 2006): (i) rifting and breakup of Rodinia (900–850 Ma); (ii) seafloor spreading (870–750 Ma) that created new oceanic lithosphere later obducted to form ophiolites (hence the term ophiolitic stage); (iii) subduction and development of arc–back-arc basins (760–650 Ma), coupled with episodes of "Older Granitoid" intrusions (760 – 610 Ma); (iv) accretion/collision marking the culmination of the Pan-African Orogeny (630 – 600 Ma); (v) continued shortening, coupled with escape tectonics and continental collapse (600 – 570 Ma); and (vi) intrusion of alkalic, post-orogenic "Younger Granites" (570 – 475 Ma).

The BIFs are hosted in volcanic to volcaniclastic/epiclastic rocks, which range in composition from basaltic to dacitic, but are mostly andesitic of calc-alkaline character. The basaltic rocks yield ages of 825 Ma (e.g. Wadi Kareim; cf. Hashad 1980), which coincide with the "ophiolitic stage" (Table 1). The island arc unit, represented by a sequence of Late Neoproterozoic volcanogenic rocks, is also known as "Shadhli metavolcanics" (Table 1; cf. Sims & James 1984; El-Gaby *et al.* 1990; Takla 2000; Basta *et al.* 2000 and references therein). This unit generally consists of (i) pyroclastics (mostly lapilli tuffs, ash fall/flow tuffs, commonly basaltic) of 712 ± 24 Ma age (e.g. Wadi Kareim; cf. Stern *et al.* 1991) and (ii) greywackes, siltstones and mudstones. The entire sequence has been affected by regional metamorphism of greenschist to amphibolite facies conditions and locally by thermal metamorphism associated with the intrusion of the "Younger" (Gattarian; post-orogenic) granites (e.g. Um Shadad and Wadi El Dabbah; Table 1; cf. Takla *et al.* 1999; Khalil 2001).

Almost all of the 13 Egyptian BIFs occur as sharply-defined stratigraphic horizons within the Neoproterozoic ophiolitic and island arc rock units, which are generally undifferentiated in most maps (e.g. Fig. 1). Only one deposit (Um Nar, # 1; Fig. 1) is suspected of being Palaeoproterozoic (El Aref *et al.* 1993). The lateral extents and thicknesses of the individual BIFs are relatively small, typically tens of meters, even if outcrops of the host rocks are widespread in the central Eastern Desert (Fig. 1). The BIFs exhibit rhythmic banding, which is either streaky (e.g. Um Ghamis) or continuous (e.g. Hadrabia), whereby layers of magnetite and hematite alternate with quartz-rich layers on macro-, meso- or micro-scales (Figs. 3a–c). Locally, the quartz-rich layers are represented by dull, red jasper consisting of microcrystalline quartz and dust-sized particles of red iron oxide (Figs. 3b, c). In some deposits, the volcaniclastic/epiclastic host rocks are also banded, retaining primary sedimentary structures such as lamination, graded bedding and load-casts. Wave-generated textures and primary structures are lacking in all deposits, although Hadrabia (#1, Fig. 1) exhibit oolitic and pisolitic textures (Essawy *et al.* 1997). The BIFs experienced strong deformation at regional- and deposit–scales as manifested by presence of folds and thrusts in the area, as well as presence of micro-folding and brecciation structures in hand specimens (Figs. 3d, e). Some deposits (e.g. Gebel Semna and Wadi Kareim) are strongly altered, often developing a porous texture (Fig. 3f).

Geological Setting of Wadi Kareim: an altered BIF

The Wadi Kareim BIF contains *c*. 17.7 Mt of iron ore reserves with an average grade of 44.6% Fe (Akaad & Abu El-Ela 2002). Its tonnage is one of the highest in the Egyptian Eastern Desert, and its average Fe grade is well above the 15–30% range of average

grades typifying most of the Egyptian BIFs. The banded iron ore reaches a thickness of 100 m and is restricted to metasedimentary layers, which were interpreted in the past as volcaniclastic rocks (El Habaak & Mahmoud 1994).

In the Wadi Kareim area, metasedimentary and metavolcanic rocks intruded by granodiorite are exposed (Fig. 4). According to Noweir *et al.* (2004), folding and regional metamorphism in this area were followed by thrusting. The metavolcanics vary from basalts to dacites but are predominantly andesitic and strongly foliated, especially in the zone of iron mineralization. The metasedimentary and metavolcanic rocks are overlain by a thick succession of conglomerates, greywackes, siltstones and mudstones belonging to the "Hammamat sediments", which are intruded by a small micro-syenite body exposed to the south of the mineralized zone (Fig. 4).

Geological Setting of Wadi El Dabbah: a "fresh" BIF

The Wadi El Dabbah deposit contains *c*. 6 Mt of ore (Dardir 1966; Akaad & Dardir 1983) hosted in metavolcanic and metasedimentary rocks that crop out in the area together with serpentinites, granitoids, and Hammamat Group sediments (Figs. 1, 5; Table 1). The BIF comprises bands ranging in thickness from a few centimeters to 10 m, and has sharp contacts with the metasediment hosts. These hosts consist of weakly metamorphosed siltstones and mudstones that have retained their primary sedimentary structures. Their beds strike N-S (Fig. 5) and conformably overlie a unit consisting mostly of meta-basalts and meta-andesites, with minor meta-tuffs, but are unconformably overlain by a thick succession of conglomerate, greywacke, siltstone, and mudstone belonging to the Hammamat Group (Table 1). The entire succession was folded into an anticline, the axis of which runs along Wadi El Dabbah, and was later affected by a steeply dipping, N-S striking normal fault with a westward down-throw. Post-tectonic ("Younger") granites, which intruded the entire section, crop out south of the area (Fig. 5). East–west striking dykes, which cut all rock units, are mostly aplitic, although some of them are trachytic or basaltic.

ANALYTICAL METHODS

Mineral chemistry

Mineral analyses for oxides in selected polished stubs and for silicates and carbonates in selected polished thin sections were performed using a CAMECA SX100 electron microprobe at the Institute of Mineralogy and Mineralogical Rohstoffe, Technical University, Clausthal, Germany. The analyses for oxides were performed at 20 kV of accelerating voltage with a specimen beam current of 40 nA whereas the silicate and carbonate analyses were performed with 20 kV accelerating voltage and 20 nA beam current, with

counting times of 20s for every analysis. Natural and synthetic minerals were used as standards. Matrix corrections were carried out using the Bence & Albee (1968) routine. Formulae for magnetite and hematite/ilmenite were calculated on the basis of three and four cations, respectively, using MINFILE (Afifi & Essene 1988). Precision is estimated at 1 – 2% of all oxide weight % values based on repeated analyses of standards. Formulae for garnet, chlorite, and stilpnomelane were calculated on the basis of 8, 10, and 7 cations, respectively. Formulae for amphiboles were calculated on the basis of 13 cations less Na, K, and Ca using AMPHIBOL (Richard & Clarke 1990). Where appropriate, Fe^{2+}/Fe^{3+} ratios were calculated based on stoichiometric constraints.

Whole rock geochemistry

Whole rock chemical analyses for the banded iron ores were carried out at the Geochemical Institute, Goettingen University, Germany, following the techniques described by Hartmann & Wedepohl (1993). Major elements, except Na_2O and K_2O, were measured from bulk rock samples using a Phillips PWI 408 XRF after fluxing the samples to form a Li-borate glass with Sr as an internal standard. Flame atomic absorption spectrometry was used to determine Na_2O and K_2O, whereas titration was used to determine FeO. Trace elements were analyzed by inductively coupled plasma atomic emission spectrometry (ICP-AES), X-ray fluorescence (Li-borate and powder pellets) and by ICP mass spectrometry. According to Hartmann & Wedepohl (1993), the precision of these techniques is typically < 0.5% or better for major elements, < 15% for minor elements, and < 30% for most trace elements. Analysis of standards yields a relative standard deviation of 1% or better for major elements, 3 – 10% for minor elements, and < 30% for most trace elements.

PETROGRAPHY

Host rock petrography

The meta-andesite, which is the most common metavolcanic rock hosting the BIFs, exhibits blastoporphyritic texture (e.g. Wadi Kareim) with phenocrysts of hornblende and plagioclase embedded in a matrix of hornblende, plagioclase, quartz, chlorite, and epidote. Titanite, ilmenite, titanomagnetite ± minor magnetite are the main accessory minerals. Hornblende (magnesio-hornblende, Table 3) is one of the most abundant minerals (modal content of *c*. 40% in Wadi Kareim and ≤90% in El Dabbah) and is commonly altered to chlorite ± epidote. Plagioclase (mainly albite-andesine) occurs as subhedral to euhedral relict phenocrysts that are variably saussuritized. Quartz occurs as fine-grained interstitial matrix crystals, or as coarser crystals filling former amygdules. Calcite ± prehnite are secondary minerals restricted to veins and amygdules. The meta-basalts/ meta-diabases consist of relict

plagioclase (highly saussuritized), and augite with metamorphic/secondary hornblende, epidote, chlorite, and titanite.

The metasedimentary rocks, which exhibit various colors (white, green, reddish-brown, and black), comprise meta-tuffs, meta-greywackes, and meta-siltstones/meta-mudstones. The meta-tuffs contain some sand-sized fragments of quartz and minor feldspars in a matrix of clay-sized quartz, feldspar ± chlorite ± sericite ± secondary (vein) calcite (e.g. Gebel Semna). The meta-greywackes are moderately to poorly sorted, and are dominated by sub-angular to sub-rounded grains of quartz, feldspars, and minor lithic fragments embedded in a silty to clayey matrix (e.g. Wadi Kareim). Quartz in these meta-greywackes occurs mostly as angular mono-crystalline grains with undulatory extinction, or as polycrystalline fragments. Feldspars occur as sub-angular grains of mostly fresh albite/oligoclase and microcline. Epidote, chlorite, and garnet are common in meta-greywackes and meta-tuffs associated with some BIFs (e.g. El Dabbah and Um Ghamis). Garnet, when present, occurs in aggregates of rounded porphyroblastic grains (≤250 μm in diameter). Opaque minerals are mainly titanohematite and Ti-rich magnetite (e.g. Wadi Kareim), or magnetite with exsolution lamellae of ilmenite (e.g. Wadi El Dabbah). Magnetite also occurs as rims surrounding Cr-rich spinels (Wadi El Dabbah; Khalil 2001).

BIF petrography

The Egyptian banded iron ores are comprised almost entirely of an oxide facies intercalated with a silicate facies. Carbonate facies, when present, consists mostly of calcite (e.g. Hadrabia, Wadi Kareim, Wadi El Dabbah), whereas sulphide facies is lacking. Magnetite is the dominant oxide facies mineral in all deposits, except at Hadrabia where hematite predominates over magnetite (Essawy *et al.* 1997). The silicate facies is characterized by quartz, hematite ± garnet ± chlorite ± stilpnomelane ± epidote. Greenalite has been reported from Hadrabia (Essawy *et al.* 1997) and Um Ghamis (Takla *et al.* 1999). However, differences in grain size, textures, and in some cases chemical compositions between oxide facies in altered and fresh banded iron ores compel separate descriptions of each type.

Petrography of altered banded iron ores

In the Wadi Kareim deposit, which exemplifies altered banded iron ores, oxide facies minerals are often porous, exhibit alternating bands enriched in magnetite, hematite, or goethite (± other limonitic material), and contain minor quartz, carbonate and pyrite. Magnetite, which typically constitutes 10–80% of the oxide facies, occurs in three textural generations: (i) magnetite I – idiomorphic very fine-grained (<20 μm) crystals, which cluster in chain-like aggregates (Fig. 6a) or are disseminated in microcrystalline quartz; (ii)

magnetite II – euhedral to subhedral medium-grained (≤125 μm) crystals (Fig. 6b); and (iii) magnetite III – anhedral to subhedral coarse-grained (≦1 mm) porphyroblasts with inclusions of quartz (Fig. 6c). Magnetites I and II are only partially altered to hematite along their rims, whereas magnetite III is often almost completely altered to martite (hematite pseudomorph after magnetite) (Figs. 6c, d), which is, in turn, partially altered to platy "specularite" (Fig. 6d). Hematite also occurs as individual fine-grained acicular crystals concentrated in bands or clusters alternating with goethite and magnetite-rich bands, or as platy crystals filling veins (Fig. 6e). Goethite concentrates in bands or fills voids between magnetite and hematite crystals giving rise to colloform texture (Fig. 6f). The porous ore is predominated by goethite with only minor hematite (Fig. 6g) and is almost devoid of quartz, which is restricted to thin veinlets cutting bands and appearing like products of compaction and desiccation.

The silicate facies consists almost entirely of quartz with minor stilpnomelane and magnetite. Quartz occurs in different forms and sizes, such as very fine-grained crystals with dust-sized Fe-oxide inclusions, medium-grained angular crystals with undulatory extinction, and coarse-grained (recrystallized?) crystals associated with coarse-grained vein calcite. Stilpnomelane occurs as stain-like material on quartz and as fine-grained laths and fibers embedded in a matrix of quartz (Fig. 6h). The carbonate facies is represented by an early generation of ankerite followed by a later generation of coarse-grained, almost pure calcite in an intricate network of anastomosing veins and veinlets. Minor amounts of Fe-rich chlorite and goethite line these veins in a few samples.

Petrography of "fresh" banded iron ores: Wadi El Dabbah/Um Nar

The Wadi El Dabbah and Um Nar deposits, which exemplify "fresh" banded iron ores, consist of alternating bands of oxide, silicate, and carbonate facies. However, unlike the altered ores, they lack pores. The oxide facies consists of alternating bands enriched in either magnetite or goethite. The magnetite-rich bands consist of dense aggregates of 10–500 μm idiomorphic to hypidiomorphic magnetite crystals and some goethite (Fig. 7a). The goethite-rich bands contain fine-grained (*c*. 30 μm) acicular hematite crystals, which are aligned with the banding and commonly concentrate in clusters, and minute (<10 μm) magnetite crystals (Figs. 7b, c). Although many magnetite crystals are partly replaced by hematite (Figs. 7a, c), complete pseudomorphic replacement of magnetite is not as common as in the altered ores at Wadi Kareim. In addition, both magnetite and hematite appear to be locally in textural equilibrium (e.g. Figs. 7b, d). Trace amounts of Fe-rich chlorite occur as an inter-granular phase between magnetite crystals, or within the goethite-rich layers.

The silicate facies ranges from millimeter-thick bands of micro-crystalline quartz with disseminated magnetite and apatite, to centimeter-thick bands of quartz, epidote, garnet, hematite, magnetite, siderite, fibrous amphibole, stilpnomelane, apatite, and minor plagioclase feldspar (Um Nar). Magnetite in the latter bands occurs in clusters surrounded by oriented hematite crystals. Garnet commonly occurs as euhedral to anhedral crystals, which are either disseminated or aggregated in quartz bands. Garnet also occurs as sizeable (0.7–1 mm) irregular porphyroblasts containing inclusions of epidote, quartz, amphibole, magnetite, and hematite (Fig. 7e). Epidote occurs as euhedral to subhedral crystals (*c*. 0.3 mm) that are either disseminated in quartz bands or cluster in aggregates, giving rise to web-like texture. Towards the contacts between the silicate and opaque-rich bands, epidote becomes coarser grained and often defines a distinct band separating garnet and quartz from hematite (Fig. 7e). Quartz and stilpnomelane display the same textural relations observed in Wadi Kareim. Amphiboles (actinolite and magnesio-hornblende) occur as subhedral to anhedral crystals, usually partially replaced by chlorite ± epidote (Wadi El Dabbah) or stilpnomelane (Um Nar). Chlorite is rare, but occurs locally as elongated flakes or fibrous aggregates, commonly with inclusions of magnetite.

MINERAL CHEMISTRY

Ore minerals

Magnetite in the banded iron ore or intercalated host rocks is almost pure, regardless of whether the ore is altered or "fresh" (Table 2). This magnetite is almost devoid of TiO_2 and typically contains <1% spinel ($MgAl_2O_4$). Despite the occurrence of three textural generations of magnetite, they are all almost chemically identical (Table 2); the main difference being a slightly higher SiO_2 for magnetite I (Table 2).

Rhombohedral oxides are mostly hematite, although ilmenite-titanohematite occurs in some metasediment-hosted banded iron ores, such as at Wadi Kareim (Table 2). Hematite (including specularite) in both "fresh" and "altered" BIF is almost pure (with <1% ilmenite). However, in altered ores, hematite pseudomorphs after magnetite III are characterized by slightly higher ilmenite component (<5%) and, overall, more impurities of CaO, Al_2O_3, and SiO_2 (Table 2).

Silicate and carbonate facies minerals

Amphibole in some deposits is either predominantly magnesio-hornblende (e.g. Wadi El Dabbah; Table 3) or ferroactinolite (e.g. Hadrabia; Essawy *et al.* 1997). The few analyses for actinolite/ferroactinolite from the banded iron ores as reported in the literature (e.g. Essawy

et al. 1997) are of poor quality and, hence, suspect. However, magnesio-hornblende is common in the host rocks of some ores as at Wadi El Dabbah (Table 3), where it is characterized by Al^{iv} = 0.9–1.35 atoms per formula unit (apfu), Al^{vi} = 0.15–0.38 apfu and <0.1 apfu Na^{M4}, calculated on the basis of 13 cations less Na, K, and Ca. Its $Fe^{2+}/(Fe^{2+} + Mg)$ ranges from 0.38 to 0.45 (Table 3).

Analyses for chlorite from fresh (e.g. Wadi El Dabbah) and altered (e.g. Gebel Semna) ores fall mainly in the ripidolite field and partly in the clinochlore field, based on Melka's (1965) classification of chlorites. Compared to chlorite in the meta-sediment hosts, chlorite in chert bands is characterized by lower Al_2O_3 (15–17 wt% versus 22–23 wt%) and higher Fe/(Fe + Mg) ratio (0.46–0.47 versus 0.23–0.24) (Table 4). Stilpnomelane has been reported from several "fresh" and "altered" deposits (e.g. Hadrabia, Essawy *et al.* 1997; Um Ghamis and Um Shaddad, Takla *et al.* 1999; Um Nar, El Aref *et al.* 1993). In Wadi Kareim, the coarse-grained fibrous variety of stilpnomelane is more aluminous and less siliceous and magnesian compared to the fine-grained, anhedral variety "staining" quartz (Table 4).

Garnet in many "fresh" banded iron ores (e.g. Wadi El Dabbah, Um Ghamis, and Um Nar) is typically un-zoned. Its composition ranges from a grossular-rich variety as in Wadi El Dabbah (average grossularite and almandine equal to 64 and 34%, respectively) with minor spessartine, pyrope, schorlomite, and goldmanite (Table 5), to a grossular-andradite-spessartine solid solution in Um Ghamis (grossularite ≅ 38%, andradite ≅ 30%, spessartine ≅ 22%, and pyrope ≅ 12%; Takla *et al.* 1999) or an almandine-rich variety in Um Nar (El Aref *et al.* 1993). In most cases, the composition of garnet in the BIFs is very close to that in the host rocks (e.g. El Dabbah, Table 5).

Apatite is common in some of the BIFs (e.g. Wadi El Dabbah). When present, apatite occurs in significant amounts and contains appreciable FeO (>1.5 wt%). Calcite is the most common carbonate in the carbonate and silicate facies, but ankerite and siderite are known in some deposits (e.g. Hadrabia; Essawy *et al.* 1997). In the BIF at Wadi Kareim, early carbonate is ankerite, whereas a later generation of coarse-grained vein carbonate is almost pure calcite with siderite component of only ≤6 mole% (Table 6). In Wadi El Dabbah, all carbonates are almost pure calcite with siderite component of <12 mole% (Table 6).

WHOLE ROCK GEOCHEMISTRY

Banded iron ores from Wadi Kareim contain 36.8–85 wt% $Fe_2O_3^T$, 11.9–40.96 wt% SiO_2, 0.6 – 2 wt% Al_2O_3, and unusually high Fe_2O_3/FeO ratios (Table 7). In contrast, banded iron ores from Wadi El Dabbah contain 27.8–70.7 wt% $Fe_2O_3^T$, 21.1–50.2 wt% SiO_2, lower Fe_2O_3/FeO ratios, and exceptionally high Al_2O_3 of 3.3–12.2 wt% (Khalil 2001). Although the Egyptian banded iron ores vary in composition from one BIF to another, the average compositions of samples from Wadi Kareim and Wadi El Dabbah are fairly representative of the altered and fresh varieties, respectively. Moreover, unpaired t-tests on Fe/Si (assuming unequal variance) reveal that both deposits are different at the 90% confidence level. This difference justifies our use of Wadi El Dabbah and Wadi Kareim BIFs as representatives of fresh and altered ores, respectively, and allows us to make some general observations on the effects of alteration. Aside from the Fe/Si ratio used as a criterion for this distinction, all fresh deposits have lower Fe^T and FeO/Fe_2O_3, and usually higher Al_2O_3 contents compared to altered deposits (Fig. 8; Table 8).

Compared to the average compositions of Algoma and Superior type BIFs of Gross & McLeod (1980) or the ranges for 215 analyses of unaltered Algoma and Superior type samples of Klein & Buekes (1993), all Egyptian BIFs are characterized by a higher Fe/Si, higher Fe_2O_3/FeO, and invariably higher Al_2O_3 contents (Fig. 8). Although the Fe/Si ratios of fresh Egyptian BIFs are not statistically different from Algoma, Lake Superior, or Rapitan type deposits as reported by Gross & McLeod (1980) and Yeo (1986), altered Egyptian BIFs show statistically significant differences in Fe/Si ratios as indicated by unpaired t-tests.

Concentrations of Cu, Ni, Cr, and V in the Wadi Kareim ore samples are broadly similar to those of Algoma type deposits, whereas those of Co and Zn are considerably lower (Tables 7 & 8; Fig. 9a). On the other hand, samples from the fresh ores in Wadi El Dabbah and Um Nar have significantly lower concentrations of most trace elements (e.g. Cr, Ni, Zn, Cu, and V) compared to average Algoma and Superior type deposits (Tables 7 & 8; Fig. 9b). Note that some Egyptian BIFs, like Um Shaddad and Um Ghamis, have concentrations of Cr, Ni, Zn, Cu, and V that are similar to those of Algoma type BIFs (Table 8; Fig. 9b; Takla *et al.* 1997), regardless of whether they are altered or fresh. Most Egyptian BIFs are also characterized by lower Sr and higher P compared to Algoma type BIFs.

Bivariate plots of trace element concentrations for Wadi Kareim BIF show that total Fe is negatively correlated with Cr and Ni (ρ = -0.12 and -0.54, respectively), but positively correlated with Cu (0.47), Zn (0.61), V (0.52) and Co (0.12). On the other hand, similar bivariate plots for samples from Wadi El Dabbah show that Fe is negatively correlated with V (-0.82), Cr (-0.27), Ni (-0.13), Co (-0.13), and Zn (-0.13), but positively correlated with Cu

(0.17). These trends and correlation coefficients for Cr, Ni, and Cu are broadly similar to the ones reported for Algoma type BIF (Gross & McLeod 1986). Nevertheless, the weakness of many of these correlations, variations in trace element concentrations/patterns from one Egyptian BIF to another, and the overall paucity of data make these generalizations dubious and risky.

Rare earth element (REE) data for the Egyptian BIFs are also scant and quite variable. The REE data for the “fresh” deposits of Gebel Hadeed, Um Nar, and Wadi El Dabbah, normalized to the North American Shale Composite (NASC) values (Condie 1993), are characterized by mild to strong HREE enrichment. For example, $(La/Yb)_{SN}$ values for BIFs at Gebel Hadeed and Um Nar fall in the range 0.1–0.2, whereas those of Wadi El Dabbah range from 0.03 to 0.04 (El Habaak & Soliman 1999). Altered deposits at Wadi Kareim show a similar HREE enrichment pattern that is slightly stronger (i.e. $(La/Yb)_{SN}$ values of 0.16–4), with occasional weak positive Eu anomalies that are somewhat similar to those of the Rapitan BIFs (El Habaak & Soliman 1999). In contrast, "fresh" ores at Um Ghamis and “altered” ores at Um Shaddad display very prominent negative Sm and positive Nd anomalies (Takla *et al.* 1999, Fig. 10), whereas the Hadrabia deposits exhibit variable REE patterns, though usually with distinct positive Eu (Eu/Eu* = 2–12) and negative Yb anomalies, and LREE enrichment when strongly oxidized (Fig. 10b; Essawy *et al.* 1997). Only BIFs at Wadi El Dabbah, Um Nar, Gebel Hadeed, and Wadi Kareim show weak negative Ce anomalies (El Habaak & Soliman 1999).

UNIQUE NATURE OF EGYPTIAN BANDED IRON FORMATIONS

The general features of the Egyptian banded iron ores compared to those classified as Algoma, Superior, and Rapitan BIF types are summarized in Table 9. These characteristics led Sims and James (1984) to suggest that the Egyptian BIFs are Algoma type deposits. Nevertheless, the Egyptian BIFs have several features that distinguish them from all types of BIFs, namely:

1. A Neoproterozoic age, in contrast to most Algoma and Superior type deposits that are typically Late Archean or Palaeoproterozoic in age (e.g. Klein 2005; Bekker *et al.* 2010). Only Um Nar is *suspected* to be of Palaeoproterozoic age (El Aref *et al.* 1993).
2. Very sharp contacts with host rocks, which are calc-alkaline metavolcanic and meta-pyroclastic rocks (e.g. Table 7) of island arc affinity. In contrast, tholeiites, shales, or diamictites are typical host rocks of Algoma, Superior, or Rapitan type BIFs, respectively.
3. Banding and lamination defined by layers of magnetite and hematite alternating with quartz-rich layers on macro-, meso- or micro-scales. Rhythmic banding is either streaky

(e.g. Um Ghamis) or continuous (e.g. Hadrabia). Wave-generated structures, common to Superior and some Rapitan type BIFs (e.g. Klein & Beukes 1993; Klein 2005) are generally lacking.

4. An oxide facies with predominant primary magnetite and minor hematite, in contrast to the predominance of primary hematite in oxides facies jaspilites of Neoproterozoic Rapitan/Urucum type BIFs.
5. Lack of a sulfide facies, and minor occurrence of carbonate facies minerals. Secondary calcite is more abundant than primary siderite or ankerite in most samples. The well-developed silicate facies contains quartz, hematite, chlorite ± stilpnomelane ± epidote ± garnet ± apatite. Greenalite was reported from Hadrabia (Essawy *et al.* 1997) whereas minnesotaite was reported from Um Nar (El Aref *et al.* 1993). These assemblages contrast with common BIF mineral assemblages where greenalite and minnesotaite, two minerals characteristic of diagenetic to low grade metamorphic conditions, do not coexist stably with hematite (Klein 1973, 2005).
6. Garnet in many Egyptian BIFs is grossular-rich and pyrope-poor (Table 5), and in some cases free of almandine (Khalil 2001; Takla *et al.* 1999). In contrast, garnets from Algoma or Superior BIFs are typically almandine-spessartine solid solutions (e.g. Klein and Beukes 1993a; Mücke *et al.* 1996).
7. Amphibole in many Egyptian BIFs is a magnesio-hornblende, and rarely a ferroactinolite (e.g. Essawy *et al.* 1997; Takla *et al.* 1999; Khalil 2001), rather than cummingtonite-grunerite, which characterizes medium-grade Algoma and Lake Superior type BIFs (e.g. Klein 2005).
8. Chlorite in all Egyptian BIFs is clinochlore-ripidolite with significantly higher Mg/(Fe + Mg) ratios (0.5–0.7) compared to Algoma and Superior type BIFs (Table 4; Fig. 11).
9. An unusually high Fe/Si ratio (Fig. 2), as well as higher Fe^{3+}/Fe^{2+} ratios for all deposits compared to Algoma and Superior types (Fig. 8). Fe/Si is considerably higher for Egyptian BIFs affected by alteration (hydrothermal or weathering?) compared to the fresh deposits.
10. Considerable variation in trace element concentrations from one deposit to another. Nevertheless, many deposits are characterized by high Al and low Cr and Ni compared to Algoma type BIFs (Table 8; Figs. 8, 9).
11. NASC-normalized REE patterns vary from one deposit to another, but generally show slight HREE enrichment in most Egyptian BIFs (cf. El Habaak & Soliman 1999), bearing some similarity to those of Rapitan type deposits and to seawater signature (e.g. Klein 2005).
12. “Fresh” Um Ghamis and “altered” Um Shaddad deposits have prominent negative Sm and positive Nd and Eu anomalies (Takla *et al.* 1999), whereas samples from Hadrabia

show vastly differing REE patterns, some of which are characterized by a slight positive Eu anomaly and LREE enrichment (Essawy *et al.* 1997; Fig. 10). In contrast, Algoma and Superior type BIFs are characterized by positive Eu anomalies, whereas Rapitan type deposits show HREE enriched patterns similar to those of modern day ocean water (e.g. Klein 2005).

The sizes, thicknesses, mineralogical compositions, associations with volcanic rocks of the individual Egyptian BIFs and general lack of granular/oolitic ores permit their classification as Algoma type deposits (e.g. Sims & James 1984). However, the Neoproterozoic age of these deposits, coupled with some of their major and trace element characteristics favor their classification as Rapitan/ Urucum type BIFs, particularly because a glaciogenic model for their formation would offer a reasonable explanation for the precipitation of Fe^{2+} bearing minerals after the GOE. However, the Neoproterozoic Rapitan/Urucum type deposits are typically jaspilites, and are associated with glacial deposits, whereas the Egyptian BIFs contain mainly magnetite and partly hematite, and their host rocks are largely devoid of diamictites (with the notable exception of Stern *et al.'s* (2006) report in Wadi Kareim).

Another intriguing feature of the Egyptian BIFs is their intercalations with volcaniclastic rocks (particularly meta-tuffs of calc-alkalic character), as opposed to the intercalation of Algoma type BIFs with tholeiitic volcanic rocks. This host-rock feature of the Egyptian BIFs suggests that they formed along an active convergent plate boundary (island arc setting?), like the formational setting of the metamorphosed BIF in the Nogolí Metamorphic Complex of the Eastern Sierras Pampeanas, Argentina (Gonzalez *et al.* 2009), in contrast with the stable continental shelf settings that have been envisioned for traditional models of BIFs (cf. James 1954; Klein and Beukes 1993a; Klein 2005). Formation of the Egyptian BIFs along an active convergent plate boundary is supported also by their relatively low Cr, Ni ± Co ± V, and high Al contents. In this setting, arc volcanism rather than intra-basinal tholeiitic volcanism may have supplied small depositional basins with significant amounts of Al and Ca, and may have contributed to the Fe and silica that are necessary for the formation of banded iron ores. This would also explain to some extent the unusual chemical compositions of garnet, chlorite, and amphibole in the silicate facies, as their precursors were characterized by relatively low Fe/Al and Fe/Mg ratios compared to other typical Algoma type deposit silicates.

The high Fe/Si ratio of the Egyptian BIFs is another unique feature. An unusually high Fe/Si ratio can be explained by post-depositional hydrothermal alteration and/or weathering by high pH ($\geq$ 8) aqueous solutions that would leach SiO_2 (e.g. Knauss & Wolery 1988). Many of the Egyptian deposits with Fe/Si > 3 show clear evidence of weathering (represented by a porous

texture) or hydrothermal alteration (represented by late veins). However, a high Fe/Si ratio could have also been a primary feature reflecting conditions of chemical sedimentation and/or diagenesis for at least some of these BIFs in which iron oxides are more abundant than interbedded chert. For example, Lascelles (2006) has shown that chert-free BIF from Mt. Gibson likely evolved by dehydration, diffusion and escape of colloidal silica through fractures during compaction. Veinlets of quartz that cross-cut ore bands in some of the Egyptian BIFs likely represent vestiges of such compaction fractures whereas chert bands that alternate with iron-oxide-rich bands represent the sinks of this colloidal silica.

The REE patterns of many fresh ores, like Um Nar and Gebel Hadeed, and altered ores, like Wadi Kareim, exhibit NASC-normalized HREE enrichment patterns (Fig. 10), which are roughly similar to patterns in the Rapitan and Urucum types of BIFs (cf. Derry & Jacobsen 1999; Klein 2005). These HREE enrichment patterns are typically interpreted as indicative of precipitation of iron oxy-hydroxides from sea water mixing with hydrothermal solutions generated close to ridge axes or submarine vents. Because metal oxy-hydroxides preferentially incorporate LREE, they cause oceanic water to become LREE-depleted, a signature that is carried by BIFs forming from such waters away from the ridge axes (Derry & Jacobsen 1999). The weak negative Ce anomaly displayed by some Egyptian BIFs (e.g. Um Nar) suggests formation of some of these deposits in relatively oxidizing environments, from which Ce^{+4} had already been removed (scavenged by Mn-oxides; Derry & Jacobsen 1999).

In contrast to the Egyptian BIFs discussed in the preceding paragraph, the patterns of REE data of BIFs at Um Shaddad and Um Ghamis (Takla et al. 1999) or at Hadrabia (Essawy *et al.* 1997) are enigmatic. Whereas strong positive Eu anomalies in Precambrian BIFs suggest considerable contribution of reducing hydrothermal solutions enriched in Eu^{2+} (Derry & Jacobsen 1999), the LREE-enriched patterns of strongly altered Hadrabia samples are unusual, and may have resulted from late alteration by cooler hydrothermal fluids that introduced the LREE without leaching out the HREE. Lastly, the strong positive Nd and negative Sm anomalies in BIFs at Um Ghamis (“fresh”) and Um Shaddad (“altered”) require either (i) fractionation of Sm from Nd by some phase during the formation of the oxide facies (possibly the scavenging of Sm by silicates like garnet that are not part of the BIF) or (ii) mixing of some oxide facies with unusual (significantly older?) sediments with high Nd/Sm ratios, which is highly unlikely because the NASC values represent averages of REEs in shales of various ages and compositions. Because interpretations of three different genetic processes for one BIF are unwieldy, one would cast doubt on the REE data for Um Ghamis and Um Shaddad (Takla *et al.* 1999) and Hadrabia (Essawy *et al.* 1993).

ORIGIN OF THE EGYPTIAN BANDED IRON FORMATIONS

Source materials and environment of deposition

The differences in mineralogy, chemistry, and texture of the Egyptian BIFs on one hand, and their associated host rocks on the other, coupled with the sharp contacts between both rock types, suggest that there was more than one source for these contrasting lithologies. The volcaniclastic rocks hosting the BIFs were likely derived predominantly from a continental/island arc source, but were delivered as detrital material to one or more marine basins where the Egyptian BIFs formed. The angular texture and poorly sorted nature of the volcaniclastic host rocks suggest a relatively short distance of transport and/or possible effect of density currents (e.g. Lascelles 2007). In contrast, the BIFs represent deposits formed *in situ* by direct precipitation from seawater, as indicated by the HREE-enriched patterns of BIFs at Gebel Hadeed, Um Nar, Wadi Kareim, and Wadi El Dabbah (El Habaak & Soliman 1999), which are similar to REE patterns of seawater (e.g. Klein & Beukes 1993b; Klein 2005).

The source of iron and silica in BIFs is typically attributed to (i) anoxic weathering on continents (e.g. Derry & Jacobsen 1990), (ii) sea floor volcanic activity, or hydrothermal vent activity on the ocean floor within their depositional basins (e.g. Trendall & Blockley 1970; Isley & Abbott 1999; Krapez *et al.* 2003), or (iii) hydrothermal leaching of pre-existing sediments (e.g. Holland 1973). In the case of the Egyptian BIFs, anoxic weathering of the continents can be ruled out, because these Neoproterozoic deposits had formed after the GOE. In addition, feldspars in the volcaniclastic host rocks are mostly fresh rather than kaolinitized/saussuritized as is typical of extensively weathered rocks. Seafloor volcanic activity, although plausible, would require that the BIFs be intercalated with tholeiitic basalts, which is not the case with the Egyptian BIFs. Hydrothermal vent activity is, however, the most likely main source of iron and silica for the Egyptian BIFs. This inference is supported by the REE patterns of most deposits, which are consistent with formation from reducing hydrothermal solutions away from ridge axes (e.g. Ruhlin & Owen 1986), and the fact that all Egyptian BIFs (except at El Dabbah) plot in the SiO_2–Al_2O_3 field of hydrothermal deposits (Wonder *et al.* 1988; Fig. 12). In most cases, temperatures of hydrothermal fluids exceeded 250ºC because most hydrothermal deposits have chondrite normalized Eu values of 4–6 (McDonough & Sun 1995; Bau & Dulski 1999) but probably remained below 400ºC to account for their low Cu contents. However, the NASC normalized Eu/Sm values of >1, Sm/Yb values of 0.017–0.4 (El-Habaak & Soliman 1999), and the chondrite normalized La/Sm values of >1 (typically 1.2–5, but with values as high as 18), are all similar to

591 respective values reported for Precambrian BIFs with no detrital/volcanic input (e.g.
592 Gonzalez *et al.* 2009 and references therein). This comparison leads us to conclude that
593 Egyptian BIFs formed by precipitation of ferroso-ferric hydroxides and hydrous iron silicates
594 from medium-temperature hydrothermal fluids, which were diluted by seawater in basins
595 receiving detrital sediment from a continent.
596
597 Distinct depositional environments have been proposed for banded iron ores, namely
598 continental shelf or deep marine (e.g. Beukes & Klein 1990; Rickard *et al.* 2004), evaporitic
599 barred basins (Button 1976), or intra-cratonic basins (Eriksson & Truswell 1978). Regardless
600 of the type of depositional environment, the distribution of iron minerals is a function of
601 specific Eh–pH conditions and stabilities of iron species, and is therefore quite predictable
602 (e.g. Drever 1974). Accordingly, sulfides are expected to form in the deepest part of the
603 basin followed successively by siderite, ferrous silicates, magnetite and hematite, as the
604 basin becomes progressively shallower (e.g. James 1954). However, this distribution pattern
605 does not apply to many BIF deposits. In fact, a reverse facies distribution has been reported
606 (e.g. Kimberly 1989; Morris & Horwitz 1983). Such reverse facies distributions have been
607 attributed to regressive-transgressive cycles and upwelling and mixing of stratified water
608 columns, as in the case of granular iron formations of the Superior type (e.g. Klein 2005).
609
610 The presence of laminations and absence of wave-generated structures in the Egyptian BIFs
611 indicate sub-aqueous precipitation below the wave base. Mineralogically, and in agreement
612 with the distribution pattern of Drever (1974) and the phase diagram of Berner (1971), the
613 formation of early magnetite as the most abundant mineral instead of hematite indicates
614 precipitation away from the shore under slightly euxinic conditions, in basins where sulfur
615 fugacities and CO_2 activities were low. Following the conventional BIF facies distribution
616 model of James (1954), the paucity of sulfide facies minerals and siderite in the Egyptian
617 BIFs would support, therefore, precipitation of iron ore precursors at some moderate depth
618 away from both the shore and basinal depo-centers. Accordingly, we suggest that the
619 Egyptian BIFs were most likely deposited in several small isolated fore-arc and back-arc
620 basins with restricted circulation and considerable submarine volcanism/hydrothermal
621 activity. Although each of these basins has had its own history that is ultimately reflected by
622 some unique features in the banded iron ores (e.g. strong Ce or Eu anomalies for some
623 deposits; Fig. 10), all basins share some common attributes that can lead us to some
624 generalizations. The intercalation of the Egyptian BIFs with poorly sorted volcaniclastic units
625 carrying angular clasts, and the high Al_2O_3 content of the BIFs suggest deposition in an
626 environment within the reach of epiclastic influx. However, the laminated nature of the BIFs
627 and the lack of wave-generated structures indicate deposition below wave base (e.g., depths

628 of >200 m). To reconcile these seemingly contradicting deductions, we suggest that the
629 volcanic arcs were relatively immature (i.e. formed by shallow-angle subduction) and had
630 rugged, steep slopes. Episodic volcanic activity within those immature volcanic arcs resulted
631 in precipitation of iron ores by ongoing hydrothermal venting in the basins during periods of
632 relative arc quiescence. The hydrothermal fluids linked with episodic volcanic activity
633 supplied the basin waters with iron and silica, but were diluted substantially by seawater
634 (which would account for the weak positive Eu anomalies in most of the BIFs). Low oxidation
635 levels within those basinal waters were achieved and sustained either through the
636 prevalence of glacial conditions, or through the delivery of volcanic dust resulting in either
637 reduction of photolytic oxidation of surface water or inhibition of growth of photosynthetic
638 organisms (e.g. Beukes & Klein 1992). Mixing of hydrothermal plume waters with cooler,
639 more oxidized waters at shallower depths nearer to the rugged shores of the volcanic islands
640 resulted in the precipitation of colloidal silica, hydrous iron silicate and insoluble ferroso-ferric
641 hydroxides as precursors to the BIF.
642
643 **Post-depositional changes: diagenesis, metamorphism and alteration**
644 Textural relations in the oxide facies of the Egyptian BIFs suggest that magnetite preceded
645 the formation of hematite (Figs. 6, 7), and that some of the textural generations of magnetite
646 (e.g. magnetite III, Wadi Kareim; Fig. 6c) formed by grain coarsening due to metamorphism.
647 The abundance of calcite and quartz veinlets in both the BIF bands and the inter-layered
648 host rocks indicates that Ca^{2+}, CO_2 and SiO_2 were all mobilized after original deposition, and
649 probably precipitated during diagenesis, metamorphism, or hydrothermal alteration. Garnet
650 is another metamorphic mineral stabilized by the relatively high Al content of the BIFs,
651 although their low pyrope and significant andradite attest to a chemical precipitate as a
652 precursor for its host rock. Nevertheless, siderite, although minor, is suspected to be
653 primary, whereas stilpnomelane is generally considered diagenetic.
654
655 Based on these textural relations, we suggest that fine-grained magnetite and quartz (or in a
656 few cases hematite + quartz) crystallized out of the hydrous Fe-silicate gel during submarine
657 diagenesis. Stilpnomelane ± chlorite ± siderite/ankerite also formed likely by diagenesis.
658 Compaction led to partial loss of silica (e.g. Lascelles 2006) as evidenced by thin quartz
659 veinlets across banding in some deposits (e.g. Wadi Kareim), and the subsequent increase
660 in Fe/Si. Low to medium-grade metamorphism (greenschist to amphibolites facies)
661 associated with the Pan-African orogeny resulted mostly in grain coarsening, as manifested
662 by the development of porphyroblastic magnetite, fibrous stilpnomelane (Fig. 6h), or coarse-
663 grained specularite (at the expense of diagenetic hematite?), and formation of garnet,
664 hornblende, and/or epidote in some lithologies.

Following metamorphism, martitization of magnetite took place, although often not to completion. Hence, newly formed martite/hematite co-existed with meta-stable magnetite (Figs. 6d, 7b, c). Because the transformation of magnetite into martite/hematite is commonly attributed to the influx of high pH and/or oxidizing fluids (Webb *et al.* 2003), we conclude that this process was primarily due to later hydrothermal alteration. Hydrothermal alteration by basic fluids would also account for the dissolution of silica, a further concomitant increase in Fe/Si characteristic of these BIFs, and ultimately the development of the porous textures characteristic of the altered ores (e.g. Figs. 3f, 7g).

SUMMARY AND CONCLUSIONS

Egyptian BIFs share many of the characteristics of some of the main types of BIFs, but they most closely resemble the Algoma type deposits. Features that make the Egyptian BIFs somewhat unique include their Neoproterozoic ages, association with calc-alkalic volcanic rocks, unusually high Fe/Si ratios, high Al, and low Cu, Ni and Co, compared to most Algoma type BIFs. Strong differences in mineralogy, texture, degree of alteration, whole rock major and trace element geochemistry, and even REE patterns (?) from one deposit to another, despite their occurrence in a relatively small area of the Eastern Desert of Egypt, are other intriguing characteristics of these BIFs.

Although it is clear that not all Egyptian BIFs share identical histories, they share many genetic aspects. We suggest that they all formed in several small fore-arc or back-arc basins, in which hydrothermal vent activity increased the concentration of Fe^{2+} in seawater. Primary Fe-silicate and oxide/hydroxide gels were precipitated below the wave base during periods of volcanic arc quiescence. The BIFs were deformed and metamorphosed during the culmination of the Pan-African Orogeny. Later hydrothermal alteration ± weathering affected some of the BIFs, resulting in leaching of SiO_2 and concentration of Fe in the “altered” deposits. This stage may have also led to the oxidation of some of the ores.

In spite of these generalized conclusions, several questions pertaining to the mode of formation of the Egyptian BIFs remain unanswered. Whereas the most likely source of Fe and silica is hydrothermal activity on basin floors close to active submarine vents, which is somewhat consistent with formation in back-arc basins, such a model is difficult to reconcile with fore-arc basin precipitation. Quantifying the contributions of hydrothermal fluid and seawater, and determining the depth of precipitation for each Egyptian BIF are therefore needed to assess the validity of the models proposed. Another issue with existing models for

the Egyptian BIFs is our inability to determine precisely the reason for low oxidation state prevailing in Neoproterozoic basins following the GOE. Serious questions remain regarding the spurious REE patterns reported in the literature for some of the Egyptian BIFs (e.g. Um Ghamis, Um Shaddad, and Hadrabia). The timing and conditions of hydrothermal alteration that affected the BIFs and caused unusually high Fe/Si ratios for some of those BIFs are poorly constrained, and reasons why the northern BIFs being altered but the southern ones remain relatively fresh are not yet established. More work is needed to fully characterize each of the Egyptian BIFs, and to address those outstanding questions.

Acknowledgements

Prof. A. Mucke is thanked for his guidance and support, and for making some of the analytical facilities used for this project available to the senior author. An insightful review by Dr. Pablo Gonzalez of an earlier draft of this manuscript helped improve this paper substantially. Dr. John Carranza is also thanked for a very critical and thorough review of the manuscript as well as his editorial handling, both of which were extremely helpful. Any remaining errors are the sole responsibility of the authors. Financial support of the U.S. National Science Foundation grant OISE 1004021 is acknowledged.

REFERENCES

ABBOTT, D. & ISLEY, A. 2001. *Oceanic upwelling and mantle plume activity: Paleomagnetic tests of ideas on the source of the Fe in early Precambrian iron formations.* In Ernst, R. E., Buchan, K. L., (eds.). Mantle plumes: their identification through time: Geological Society of America, Special Paper **352**, 323-339. Boulder, Colorado, USA.

AFIFI, A. M. & ESSENE, E. J. 1988. *MINFILE: a microcomputer program for storage and manipulation of chemical data on minerals.* American Mineralogist, **73**, 446-447.

AKAAD, M. K., & DARDIR, A. A. 1983. *Geology of Wadi El Dabbah iron ore deposits, Eastern Desert of Egypt.* Bulletin of Faculty of Earth Sciences, King Abdulaziz University, **6**, 611-617.

AKKAD, M. K., & ABU EL ELA, A. M. 2002. *Geology of the basement rocks in the Eastern half of the belt between Latitudes 25° 30 and 26° 30' N Central Eastern Desert, Egypt.* The Geological Survey of Egypt, **78**, 1-118.

AYRES, D. E. 1972. *Genesis of iron-bearing minerals in banded iron formation mesobands in the Dates Gorge Member, Hammersely Group, Western Australia.* Economic Geology, **67**, 1214-1233.

BASTA, F. F., Takla, M. A. & MAURICE, A. E. 2000. *The Abu Marawat banded iron-formation: Geology, mineralogy, geochemistry and origin.* 5th International Conference on Geology of Arab World, Cairo University, 319-334.

BAU, M., & DULSKI, P. 1999. *Comparing yttrium and rare earth in hydrothermal fluids from the Mid-Atlantic Ridge: Implications for Y and REE behavior during near vent mixing and the Y/Ho ratio of Proterozoic seawater.* Chemical Geology, **155**, 7-90.

BEKKER, A., SLACK, J. F., PLANAVSKY, N., KRAPEZ, B., HOFMANN, A., KONHAUSER, K. O., & ROUXEL, O. J. 2010. Iron Formation: *The Sedimentary Product of a Complex Interplay among Mantle, Tectonic, Oceanic, and Biospheric Processes.* Economic Geology, **105**, 467-508.

BEKIR, R. K., & NIAZY, E. A. 1997. *Magnetite ore mineralization of Um Gheig area, Eastern Desert, Egypt.* Egyptian Mineralogist, **9**, 133-145.

BENCE, A. E., & ALBEE, A. L. 1968. *Empirical correction factors for the electron microanalysis of silicates and oxides.* Journal of Geology, **76**, 382-403.

BERNER, R. A. 1971. *Principles of Chemical Sedimentology.* New York, McGraw-Hill Book Company, 240p.

BEUKES, N. J., & KLEIN, C. 1990. *Geochemistry and sedimentology of a facies transition- from microbanded to granular iron-formation- in the early Proterozoic Transvaal Supergroup, South Africa*. Precambrian Research, **47**, 99-139.

BEUKES, N. J., & KLEIN, C. 1992. *Models for iron formation deposition.* In Schopf, J. W., and Klein, C. (eds.). The Proterozoic Biosphere: A multidisciplinary study, 147-151. Cambridge University Press, New York.

BUTTON, A. 1976. *Transvaal and Hamersley Basins: Review of basin development and mineral deposits.* Mineral Science and Engineering, **8**, 262-293.

CONDIE, K. C. 1993. *Chemical composition and evolution of the upper continental crust: contrasting results from surface samples and shales.* Chemical Geology, **104**, 1-37.

DARDIR, A. A. 1966. *Geology of Wadi El Dabbah iron ore deposits, Eastern Desert, Egypt.* M.Sc. Thesis, Assuit University, Egypt.

DARDIR A. A. 1990. *Status and future development of iron and steel industry in Egypt.* Unpublished report, Geological Survey, Egypt, 22 pp.

DERRY, L. A., & JACOBSEN, S. B. 1999. *The chemical evolution of Precambrian seawater: Evidence from REEs in banded iron formations.* Geochimica et Cosmochimica Acta, **54**, 2965-2977.

DREVER, J. L. 1974. *Geochemical model for the origin of Precambrian banded iron formations.* Geological Society of America Bulletin, **85**, 1099-1106.

EGYPTIAN GEOLOGICAL SURVEY 1981. *Geological Map of Egypt.* Accessed 2010-09-03 at http://library.wur.nl/isric/kaart/origineel/afr_egg.jpg

EL AREF, M. M., EL DOUDGDOUG, A., ABDEL WAHED, M. & EL MANAWI, A. W. 1993. *Diagenetic and metamorphic history of Umm Nar BIF, Eastern Desert, Egypt.* Mineral. Deposita, **28**, 264-278.

EL-GABY, S., LIST, F. K., TEHRANI, R. 1988. *Geology, evolution and metallogenesis of the Pan-African belt in Egypt.* In: El-Gaby S., Greiling R.O., (eds.). The Pan-African belt of northeast Africa and adjacent areas. Vieweg Sohn, Braunschweig/Wiesbaden, 17-68.

EL-GABY, S., List, F. K., & TEHRANI, R. 1990. *The basement complex of the Eastern Desert and Sinai.* In Said, R., (ed.). The Geology of Egypt. Balkema, Rotterdam, 175-184.

EL HABAAK, G. H. 2005. *Sedimentary facies and depositional environments of some Egyptian banded iron-formations.* 4th International Conference on the Geology of Africa, Assiut University, Assiut, Egypt (abstract).

EL HABAAK, G. H., & MAHMOUD, S. 1994. *Carbonaceous bodies of debatable organic provenance in the Banded Iron Formation of the Wadi Kareim area, Eastern desert, Egypt.* Journal of African Earth Science, **19**, 125-133.

EL HABAAK, G. H., & SOLIMAN, M. F. 1999. *Rare earth elements geochemistry of the Egyptian banded iron-formation and evolution of the Precambrian atmosphere and ocean.* 4th International Conference on Geochemistry, Alexandria University, Egypt., 149-169.

ERIKSSON, K. A., & TRUSWELL, J. F., 1978. *Geological processes and atmospheric evolution in the Precambrian.* In Tarling, D. H. (ed.). Evolution of the Earth's crust, 219-238. Academic Press, London.

ESSAWY, M. A., ZALATA, A. A., & MAKROUM, F. 1997. *Hadrabia banded iron-formation, Eastern Desert, Egypt.* Egyptian Mineralogist, **9**, 147-168.

GARRELS, R. M., PERRY JR., E. A., & MCKENZIE, F. T. 1973. *Genesis of Precambrian iron formations and the development of atmospheric oxygen.* Economic Geology, **68**: 1173-1179.

GONZÀLEZ, P. D., SATO, A. M., LLAMBIAS, E. J., & PETRONILHO, L. A. 2009. *Petrology and Geochemistry of the banded iron formation in the eastern Sierras Pameanas of San Luis (Argentina): Implications for the evolution of the Nogolì Metamorphic Complex.* Journal of South American Earth Sciences, **28**, 89-112.

GROSS, G. A. 1965. *Geology of iron deposits in Canada. General geology and evaluation of iron deposits.* Geological Survey, Canada, Economic Geology Section, **22**, *3*, 179pp.

GROSS, G. A. 1980. *A classification of iron-formations based on depositional environments.* The Canadian Mineralogist, **18**, 215-222.

GROSS, G. A. 1996. *Algoma-type Iron-formation.* In: Lefebure, D. V. and Hoy, T. (eds.). Selected British Columbia Mineral Deposit Profiles, Volume 2 – Metallic Deposits. British Columbia Ministry of Employment and Investment, Open File **1996-13**, 25-28.

GROSS, G. A., & MCLEOD, C. R. 1980. *A preliminary assessment of the chemical composition of iron-formations in Canada.* The Canadian Mineralogist, **18**, 223-229.

HARTMANN, G. & WEDEPOHL, K. H. 1993. *The composition of peridotite tectonites from the Ivrea Complex (North Italy), residues from melt extraction.* Geochimica et Cosmochimica Acta, **57**, 1761-1782.

HASHAD, A. H. 1980. *Present status of geochronological data on the Egyptian basement complex.* Bulletin of the Institute of Applied Geology, King Abdul Aziz University, Jeddah, **3**, 31-46.

HOLLAND, H. D. 1973. *The oceans, a possible source of iron-formations.* Economic Geology, **68**, 1169-1172.

HUSTON, D. L., & LOGAN, G. A. 2004. *Barite, BIFs and bugs: evidence for the evolution of the Earth's early hydrosphere.* Earth and Planetary Science Letters, **220**, 41-55.

ISLEY, A. E., & ABBOTT, D. H. 1999. *Plume-related mafic volcanism and the deposition of banded iron-formation.* Journal of Geophysical Research, **104**, 15461-15477.

JAMES, H. L. 1954. *Sedimentary facies of iron-formation.* Economic Geology, **49**, 235-293.

JAMES, H. L. 1992. *Precambrian iron-formation: Nature, origin, and mineralogic evolution from sedimentary to metamorphism.* In: Wolf, K.H., Chiligarian, C. V., (eds.). Developments in Sedimentology, **47**, 543-589.

KHALIL, K. I. 2001. *Banded iron-formation (BIF) of Wadi El Dabbah area, Central Eastern Desert, Egypt: A genetic concept.* 5th International Conference on Geochemistry, Alexandria University, 333-352.

KHALIL K. I. 2008. *Origin and alteration of banded iron-formation (BIF) at Gebel Semna, Eastern Desert, Egypt: mineralogical and geochemical constraints.* 8th International Conference on Geochemistry, Alexandria University, Egypt. (Abstract).

KIMBERLY, M. M. 1989. *Exhalative origins of the iron-formation.* Ore Geology Review, **5**, 13-145.

KLEIN, C. 1973. *Changes in Mineral Assemblages with metamorphism of some Banded Iron Formations.* Economic Geology, **68**, 1075-1088.

KLEIN, C. 2005. Some Precambrian banded iron formations from around the world: Their age, geologic setting, mineralogy, metamorphism, geochemistry, and origin. American Mineralogist, **90**, 1473-1499.

KLEIN, C., & BEUKES, N. J. 1992. *Time distribution, stratigraphy and sedimentologic setting, and geochemistry of Precambrian Iron Formation.* In Schopf, J. W., & Klein, C. The Proterozoic Biosphere: A multidisciplinary study, 139 – 146. Cambridge University Press, New York.

KLEIN, C., & BEUKES, N. J. 1993a. *Proterozoic iron-formations.* In: Condie, K.C., (ed.). Development in Precambrian Geology: Proterozoic crustal evolution. 10, 383-418.

KLEIN, C., & BEUKES, N. J. 1993b. Sedimentology and Geochemistry of Late Proterozoic Rapitan Iron Formation in Canada. Economic Geology, **88**, 542-565.

KLEIN, C., & LADEIRA, E. A. 2004. *Geochemistry and mineralogy of Neoproterozoic banded iron-formations and some selected siliceous manganese formations from the Urucum District, Matto Grosso do Sul, Brazil.* Economic Geology, **99**, 1233-1244.

KNAUSS, K. G., & WOLREY, T. J. 1988. *The dissolution kinetics of quartz as a function of pH and time at 70°C.* Geochimica et Cosmochimica Acta, **52**, 43-53.

KRAPEZ, B., BARLEY, M. E., & PICKARD, A. L. 2003. *Hydrothermal and resedimented origin of the precursor sediments to banded iron formation: sedimentological evidence from the Early Palaeoproterozoic Brockmann Supersequence of Western Australia*. Sedimentology, **50**, 979-1011.

KRONER, , A., & STERN, R. J. 2004. *Pan-African Orogeny.* Encyclopedia of Geology, 1:1-12.

LASCELLES, D. F. 2006. *The Mt Gibson banded iron formation hosted magnetite deposit: two distinct processes for the origin of high grade iron ore deposits.* Economic Geology, **101**: 651-666.

LASCELLES, D. F. 2007. *Black smokers and density currents: A uniformatarian model for the genesis of banded iron-formations.* Ore Geol. Rev., **32**, 381-411.

LAIRD, J. 1998. *Chlorites: metamorphic petrology.* In: Bailey, S.W. (Ed.), Hydrous phyllosilicates. Reviews in Mineralogy, **19**, 405-447.

MCDONOUGH, W. F. & Sun, S. -S. 1995. *Composition of the Earth.* Chemical Geology, **120**, 223-253.

MELKA, K. 1965. *Proposal of chlorite classification.* Vestnik Ustredniho Ustavu Geologie, **40**, 23-29.

MORRIS, R. C., & HORWITZ, R. C. 1983. *The origin of the iron formation rich Hamersely Group of Western Australia – Deposition on a Platform.* Precambrian Research, **21**, 273-297.

MÜCKE, A., ANNOR, A., NEUMANN, U. 1996. *The Algoma-type iron-formations of the Nigerian metavolcano-sedimentary schist belts.* Mineralium Deposita, **31**, 113-122.

NOWEIR, M. A., GHONEIM, M. F., ABU ALAM, & T. S. 2004. *Structural framework and geochemical studies of iron-ore deposits of Wadi Kareim, Central Eastern Desert, Egypt.* 6th International Conference on Geochemistry, Alexandria University. Egypt, I-B, 821-847.

RICHARD, L. R. & CLARKE, D. B. 1990. *AMPHIBOL: A program for calculating structural formulae and for classifying and plotting chemical analyses of amphiboles.* American Mineralogist, **75**, 421-423.

RICKARD, A. L., BARLEY, M. E. & KRAPEZ, B. 2004. *Deep-marine depositional setting of banded iron formation: sedimentological evidence from interbedded clastic sedimentary rocks in the early Palaeoproterozoic Dales George Member of Western Australia.* Sedimentary Geology, **170**, 37-62.

RUHLIN, D. E., & OWEN, R. M. 1986. *The rare earth element geochemistry of hydrothermal sediments from the East Pacific Rise: Examination of seawater scavenging mechanism.* Geochimica et Cosmochimica Acta, **50**, 393-400.

SALEM, A., & EL- SHIBINY, N. H. 2002. *Contribution to the mineralogy, geochemistry and genesis of iron deposits from Wadi Kareim, Eastern Desert, Egypt.* Delta Journal of Science, **26**, 129-147.

SALEM, A. K., NIAZY, E. A., & KAMEL, O. A. 1994. *New occurrence of contact metasomatic iron ores in El Imra area, Eastern Desert, Egypt: its mineralogy and origin.* Egyptian Mineralogist, **6**, 53-75.

SHEIKHIKHOU, H. 1992. *Erzmikroskopische und mikrosondenanalytische untersuchung der lagerstätte Gole Gohar/Iran und deren Vergleich mit den Kiruna Type magnetit-Lagerstätten: Kiruna/Schweder, Bafg/Iran, Avnik/Türei, El Laco/Chile Sowie den Lagerstätte Phallaborwa/SA und Kovder/Russland.* Unpublished diplom Thesis, University Goettingen, 114 pp.

SIMONSON, B. M. 2003. *Origin and evolution of large Precambrian iron formations.* In Chan, M. A., and Archer, A. W. (eds.). Extreme depositional environments: Mega end members in geological time. Geological Society of America Special Paper **370**, 231-244. Boulder, Colorado, USA.

SIMS, M. A., & JAMES, H. L. 1984. *Banded iron ore formation of Late Proterozoic age in the Central Eastern desert, Egypt: geological and tectonic setting.* Economic Geology, **79**, 1777-1784.

STERN, R. J., KRÖNER, A. & RASHWAN, A. A. 1991. *A Late Precambrian (~ 710Ma) high volcanicity rift in the South Eastern Desert of Egypt.* Geolische Rundschau, **80**, 155-170.

STERN, R. J., AVIGAD, D., MILLER, N. R, & BEYTH, M. 2006. *Evidence for snowball earth hypothesis in the Arabian-Nubian Shield and the East African orogen.* Journal of African Earth Sciences, 44, 1-20.

TAKLA, M. A. 2000. *Tectonic evolution and mineralization of the Arabo-Nubian massif. Invited talk, 5th International Conference on Geology of Arab World, Cairo University, Egypt.*

TAKLA, M. A., HAMIMI, Z., HASSANEIN, S. M., & KAOUD, N. N. 1999. *Characterization and genesis of the BIF associating arc metavolcanics, Umm Ghamis area, Central Eastern Desert Egypt.* Egyptian Mineralogist, **11**, 157-185.

TRENDALL, A. F., & BLOCKLEY, J. G. 1970. *The iron formations of the Precambrian Hamersley Group of Western Australia, with special reference to crocidolite. Western Australia*. Geological Survey Bulletin, **119**, 353 pp.

WEBB, A. D., DICKENS, G. R. & OLIVER, N. H. S. 2003. *From banded iron-formation to iron ore: geochemical and mineralogical constraints from across the Hamersley Province, Western Australia.* Chemical Geology, **197**, 215-251.

WONDER, J., SPRY, P., & WINDOM, K. 1988. *Geochemistry and origin of manganese-rich rocks related to iron-formation and sulfide deposits, western Georgia.* Economic Geology, **83**, 1070 - 1081.

YEO, G. M. 1986. *Iron-formation in the Late Proterozoic Rapitian Group, Yukon and Northwest Territories.* In: Morin, J.A. (Ed.), Mineral Deposits of the Northern Cordillera. Canadian Institute of Mineralogy and Metallurgy Special Volume, **37**, 142-153.

Figure Captions

Fig. 1. Simplified geological map of Egypt (modified after El Gaby *et al.* 1990) showing the locations of 13 banded iron-ores (open circles). Inset is a simplified lithological map of the area outlined in the box (simplified from Egyptian Geological Survey 1981). Archean/L. Proterozoic (undiff.) represents undifferentiated Archean to Lower Proterozoic rocks (cf. Table 1 for more details).

Fig. 2. Bulk rock compositions of "Fresh" and "Altered" BIFs from Egypt relative to Algoma, Superior, and Rapitan average compositions from Gross & McLeod (1980), plotted on a Si–Fe diagram.

Fig. 3. Main features of Egyptian BIFs: (a) Macro- and meso- scale banding in one of the least altered BIF samples from Gebel Semna (altered BIF). (b) Meso- and (c) micro-scale banding (lamination) between alternating jasper (red) and Fe-ore in unaltered samples from Wadi Kareim (altered BIF). (d) Strong folding and (e) brecciation of chert in oxide facies samples from Um Nar (Fresh BIF). (f) Altered sample with a highly porous texture from Gebel Semna.

Fig. 4. Simplified geological map of Wadi Kareim area (deposit # 5, Fig. 1; modified from El Habaak & Mahmoud (1994) and Noweir *et al.* (2004)). Banded iron ores occur within the metasedimentary units indicated as "Fe-bearing metasediments".

Fig. 5. Simplified geological map of Wadi El Dabbah area (deposit # 6, Fig. 1; modified after Akkad and Dardir (1983)). The banded iron ore occurs within the unit indicated as "Metasediments".

Fig. 6. Photomicrographs showing selected textural relations from Wadi Kareim. (a) Fine-grained early "magnetite I" embedded in ultrafine-grained quartz (OIPRL). (b) Relicts of early? "magnetite II" (Mgt; grey tone) replaced by martite/hematite (bright tone) (OIPRL). (c) Coarse-grained porphyroblasts of strongly martitized magnetite preserved as relicts (arrow) (OIPRL). (d) Relict of strongly martitized magnetite, and transformed into platy specular hematite (Hm) (OIPRL). (e) Alternating bands enriched in goethite (dark grey) and hematite (white) crosscut by a vein of specular hematite lined with minor quartz (black) and goethite (PRL). (f) Colloform banding of goethite (Gth) and other limonitic material filling in spaces between coarse-grained hematite (Hm), magnetite (partly replaced by hematite along rims, and quartz (PRL) (g) Porous ore predominated by goethite with stringers of very fine-grained hematite (PRL). (h) Fibrous stilpnomelane (Stp) in silicate facies (PPTL). Abbreviations: OIPRL = oil immersion polarized reflected light; PRL = polarized reflected light' PPTL = plane polarized transmitted light.

Fig. 7. Photomicrographs showing selected textural relations from Wadi El-Dabbah (a – c) and Um Nar (d – f). (a) Subhedral magnetite crystals (brownish grey) partly replaced by hematite (white) in magnetite-rich band (PRL). (b) Goethite (Gth), hematite (Hm) and magnetite (Mgt) in goethite-rich band (PRL). (c) Clusters of hematite (Hm) and fine-grained magnetite (Mgt) rimmed by hematite in goethite-rich bands (PRL). (d) Magnetite (Mgt) and hematite (Hm) in apparent textural equilibrium in silicate facies band (PRL). (e) Epidote-rich band separating garnet + quartz rich band from hematite + magnetite rich oxide facies band (PPTL). (h) Fibrous amphibole inter-grown with magnetite, epidote and quartz, silicate facies (PPTL). See Fig. 6 for explanations of abbreviations.

Fig. 8. Bulk rock major oxide components of some Egyptian banded iron ores compared to averages of major oxides in Algoma, Superior, and Rapitan type BIFs from Klein (2005). All analyses recalculated on an anhydrous, CO_2-free basis. Shaded area represents Klein's (2005) range for Algoma and Superior type BIFs.

Fig. 9. Trace element spider diagrams for BIF samples. (a) Data from Wadi Kareim (this study). (b) Averages of data from Um Nar (El Aref *et al.* 1993), W. El Dabbah (Khalil 2001), Hadrabia (Essawy *et al.* 1997); Um Shaddad (Takla *et al.* 1999), and Gebel Semna (Khalil 2008), and from Algoma, Superior, and Rapitan types of BIFs (Gross & McLeod 1980; Yeo 1986).

Fig. 10. REE values normalized to North American Shale Composite (NASC): (a) "fresh" BIFs at Um Ghamis (Takla *et al.*, 1999), Um Nar, Wadi El Dabbah, and Gebel Hadeed (El Habaak & Soliman 1999); (b) "altered" BIFs at Hadrabia (Essawy *et al.* 1997), Wadi Kareim (El Habaak & Soliman 1999), and Um Shaddad (Takla *et al.*, 1999).

Fig. 11. Chemical composition of chlorites in various geological environments (Laird 1988; Sheikhikhou 1992). Solid and open circles are chlorites from Gebel Semna (altered BIF) and Wadi El Dabbah (fresh BIF), respectively.

Fig. 12. Al_2O_3–SiO_2 compositions of Wadi Kareim (this study), representative Um Ghamis and average Um Shaddad (Takla *et al.*, 1999), average Um Nar (El Aref *et al.*, 1993), average Wadi El Dabbah (Khalil 2001), average Gebel Semna (Khalil 2008), and average data from Algoma, Superior, and Rapitan types of BIFs (Gross & McLeod 1980; Yeo, 1986). Al_2O_3–SiO_2 fields are from Wonder *et al.* (1988).

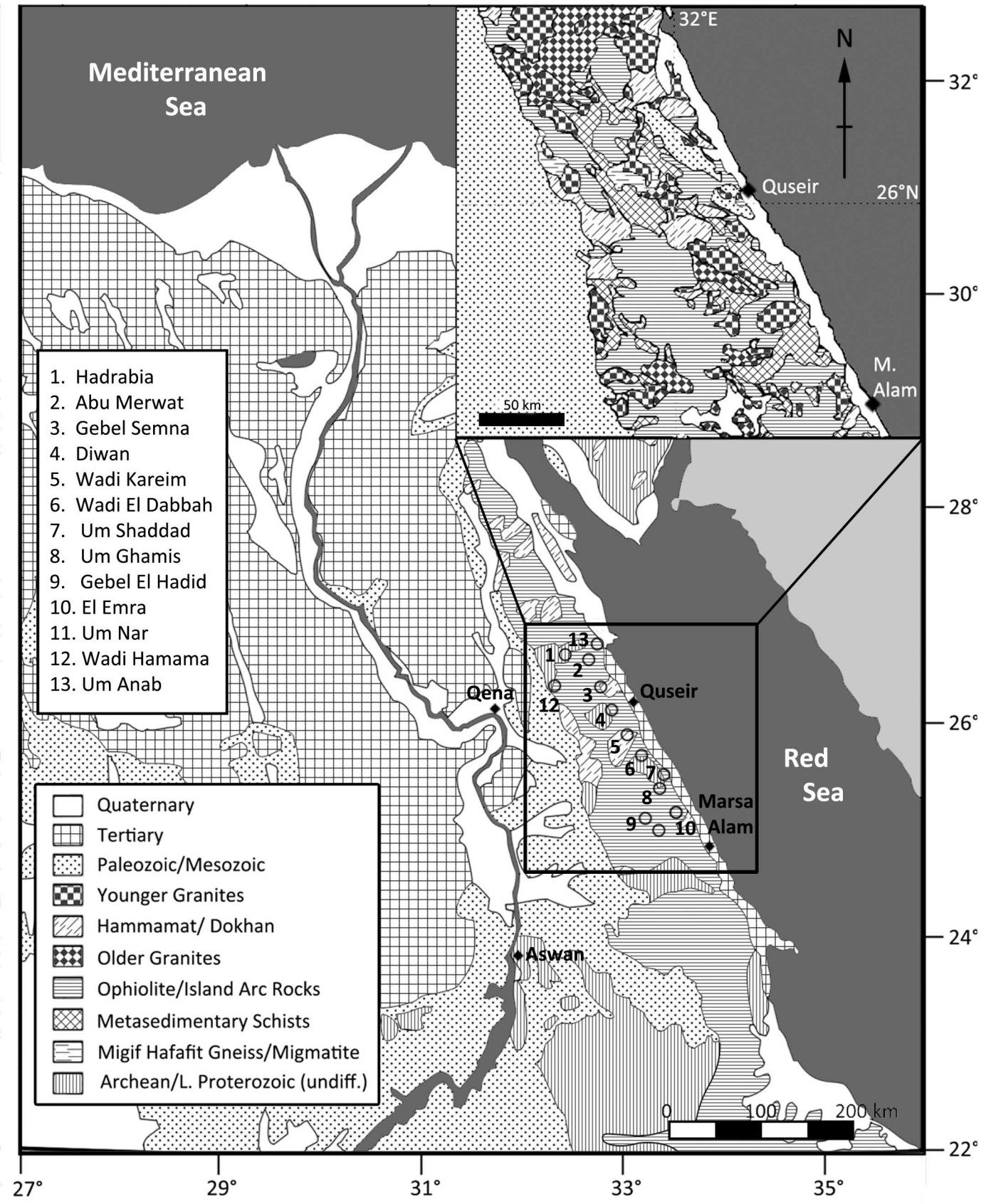
Mediterranean Sea
32°E
N
Quseir
26°N
M. Alam
50 km
1. Hadrabia
2. Abu Merwat
3. Gebel Semna
4. Diwan
5. Wadi Kareim
6. Wadi El Dabbah
7. Um Shaddad
8. Um Ghamis
9. Gebel El Hadid
10. El Emra
11. Um Nar
12. Wadi Hamama
13. Um Anab
Qena
Quseir
Marsa Alam
Red Sea
Aswan
Quaternary
Tertiary
Paleozoic/Mesozoic
Younger Granites
Hammamat/ Dokhan
Older Granites
Ophiolite/Island Arc Rocks
Metasedimentary Schists
Migif Hafafit Gneiss/Migmatite
Archean/L. Proterozoic (undiff.)
0
100
200 km
32°
30°
28°
26°
24°
22°
27°
29°
31°
33°
35°

Fig. 2

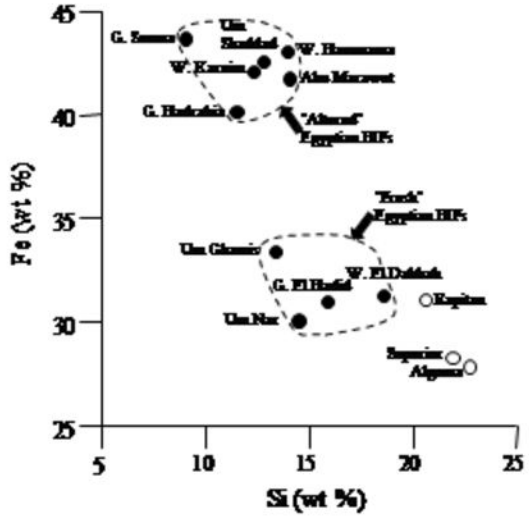

Fig. 3

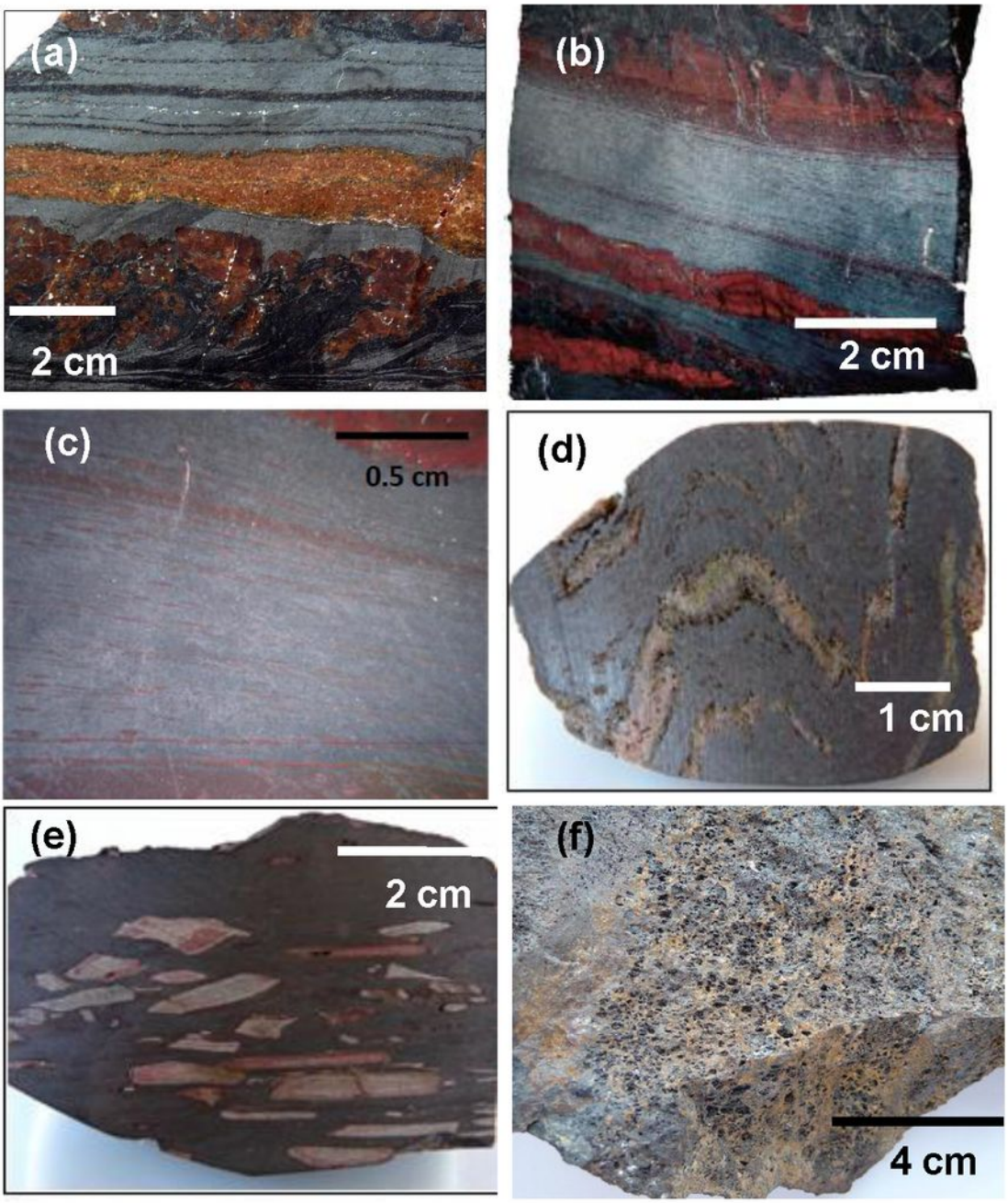

Fig. 4

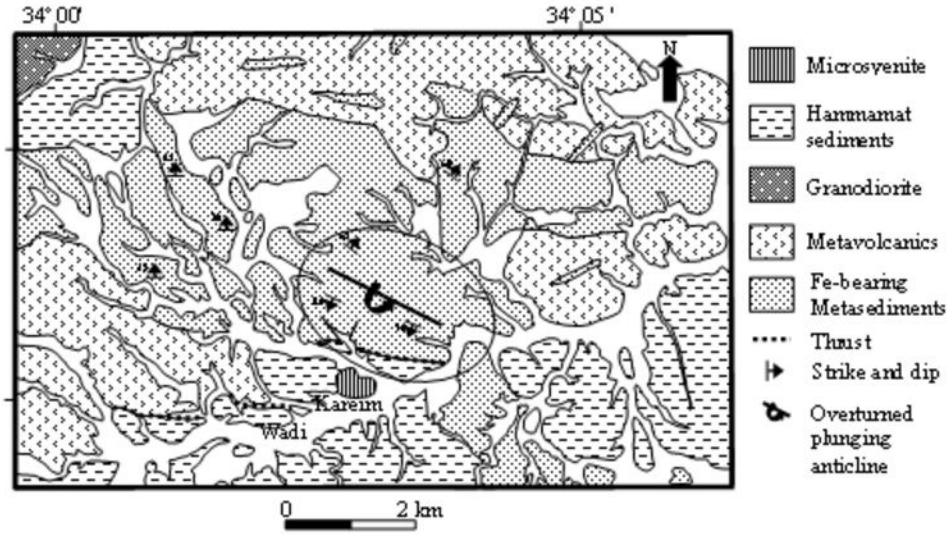
34° 00'
34° 05'
N
Karem
Wadi
0
2 km
Microsyenite
Hammamat sediments
Granodiorite
Metavolcanics
Fe-bearing Metasediments
Thrust
Strike and dip
Overturned plunging anticline

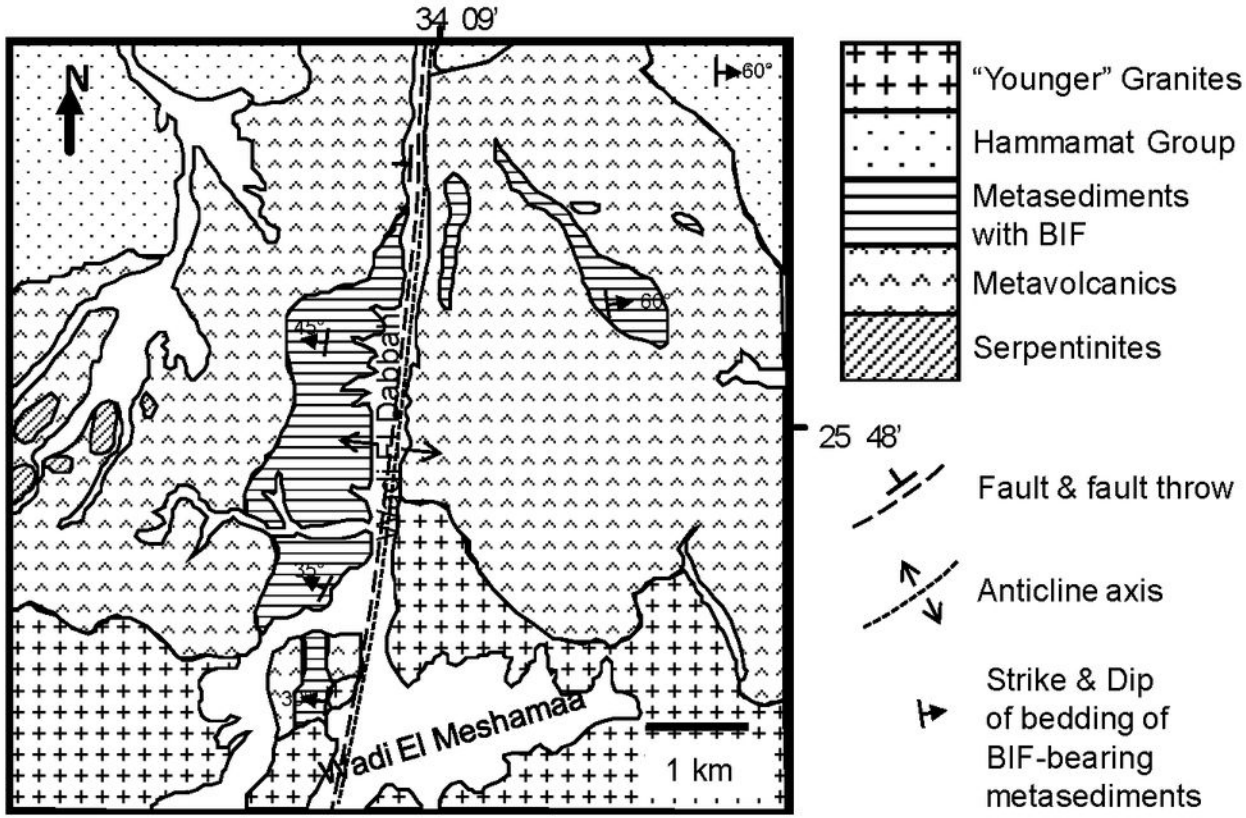
34 09'
N
60°
66°
45°
Wadi El Dabbah
Wadi El Meshamaa
1 km
25 48'
"Younger" Granites
Hammamat Group
Metasediments with BIF
Metavolcanics
Serpentinites
Fault & fault throw
Anticline axis
Strike & Dip of bedding of BIF-bearing metasediments

Fig. 6

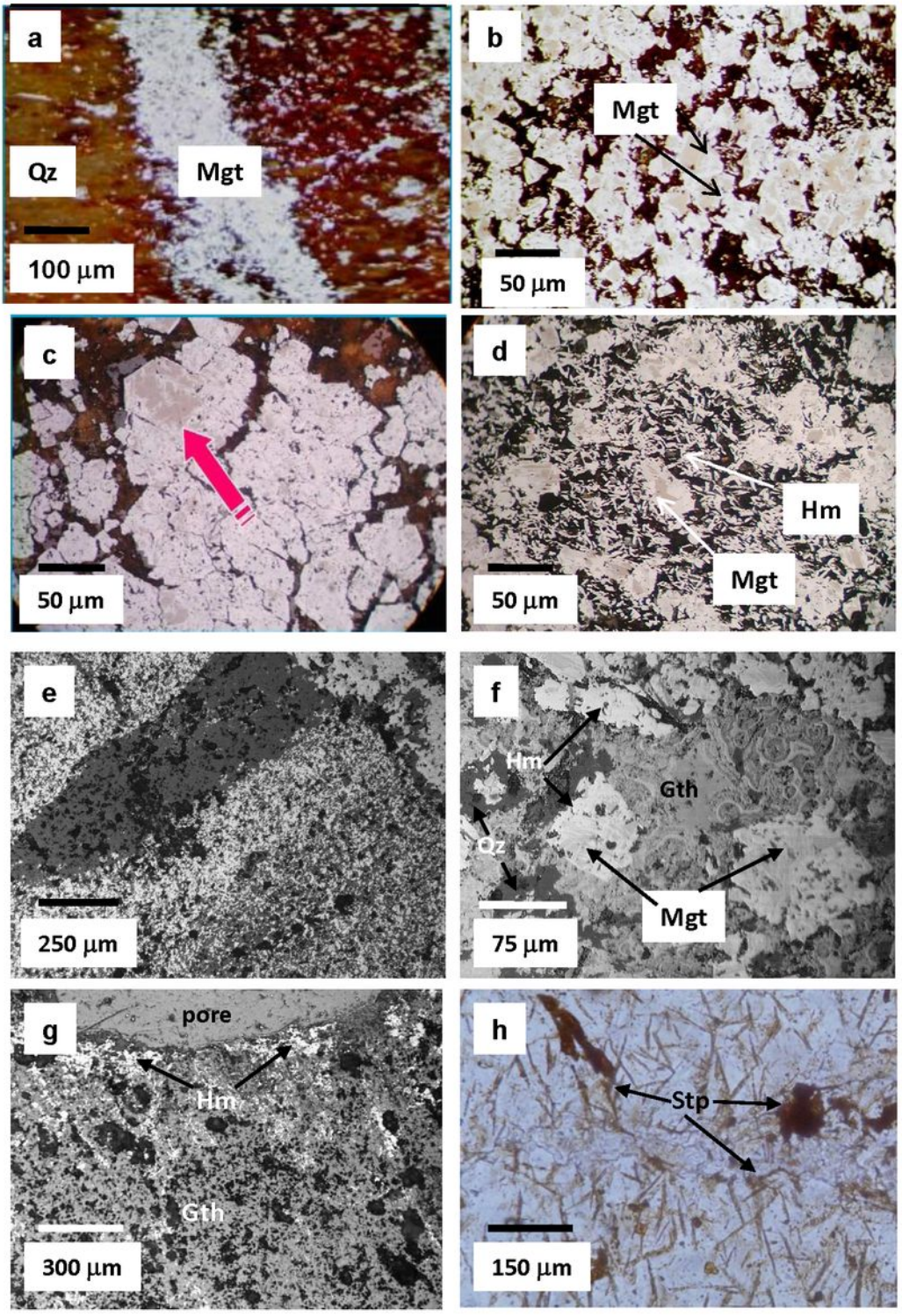
a
Qz
Mgt
100 μm
b
Mgt
50 μm
c
50 μm
d
Hm
Mgt
50 μm
e
250 μm
f
Hm
Gth
Qz
Mgt
75 μm
g
pore
Hm
Gth
300 μm
h
Stp
150 μm

Fig. 7

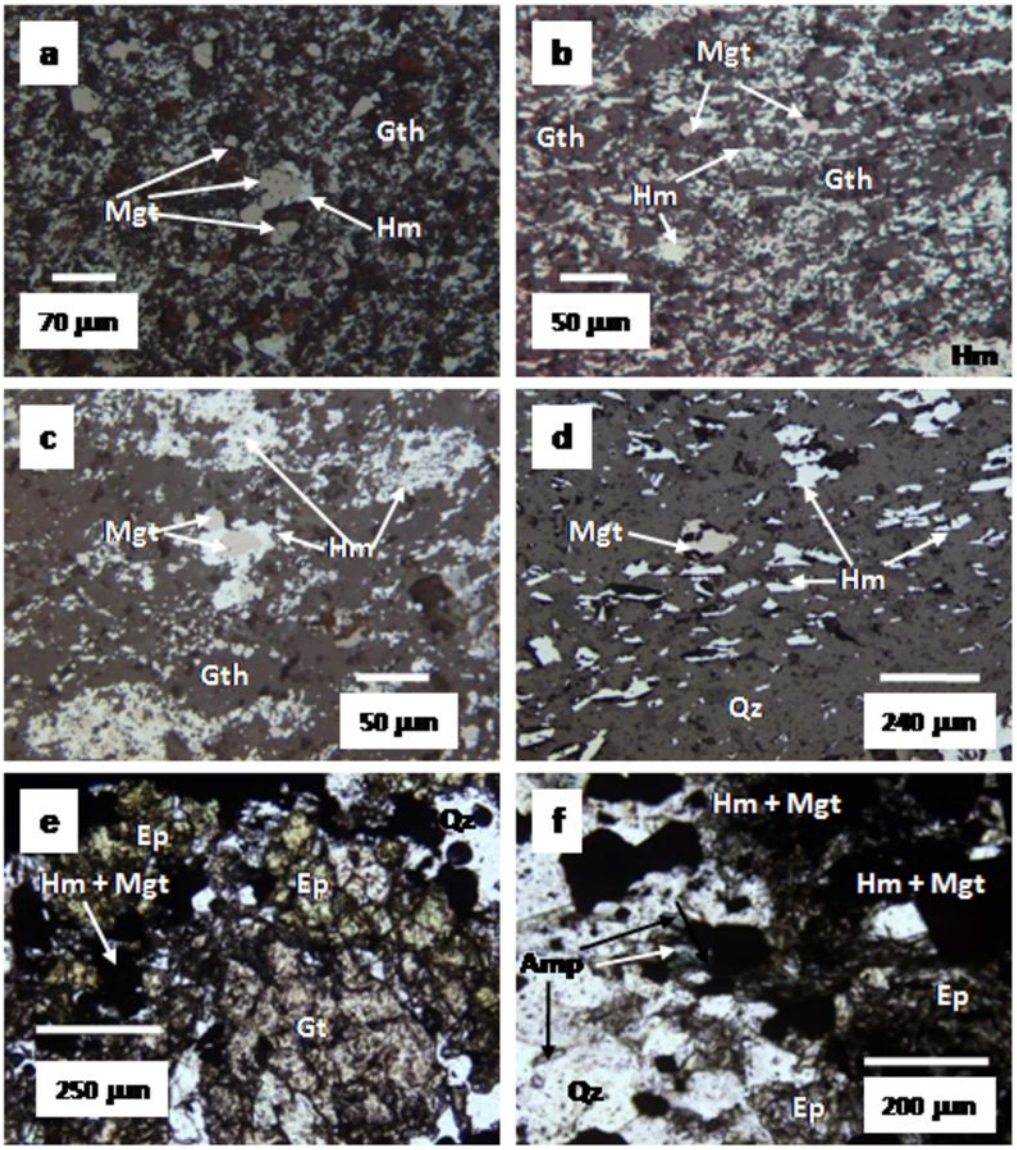
a
Gth
Mgt
Hm
70 µm
b
Mgt
Gth
Hm
Gth
50 µm
Hm
c
Mgt
Hm
Gth
50 µm
d
Mgt
Hm
Qz
240 µm
e
Ep
Qz
Hm + Mgt
Ep
Gt
250 µm
f
Hm + Mgt
Hm + Mgt
Amp
Ep
Qz
Ep
200 µm

Fig. 8

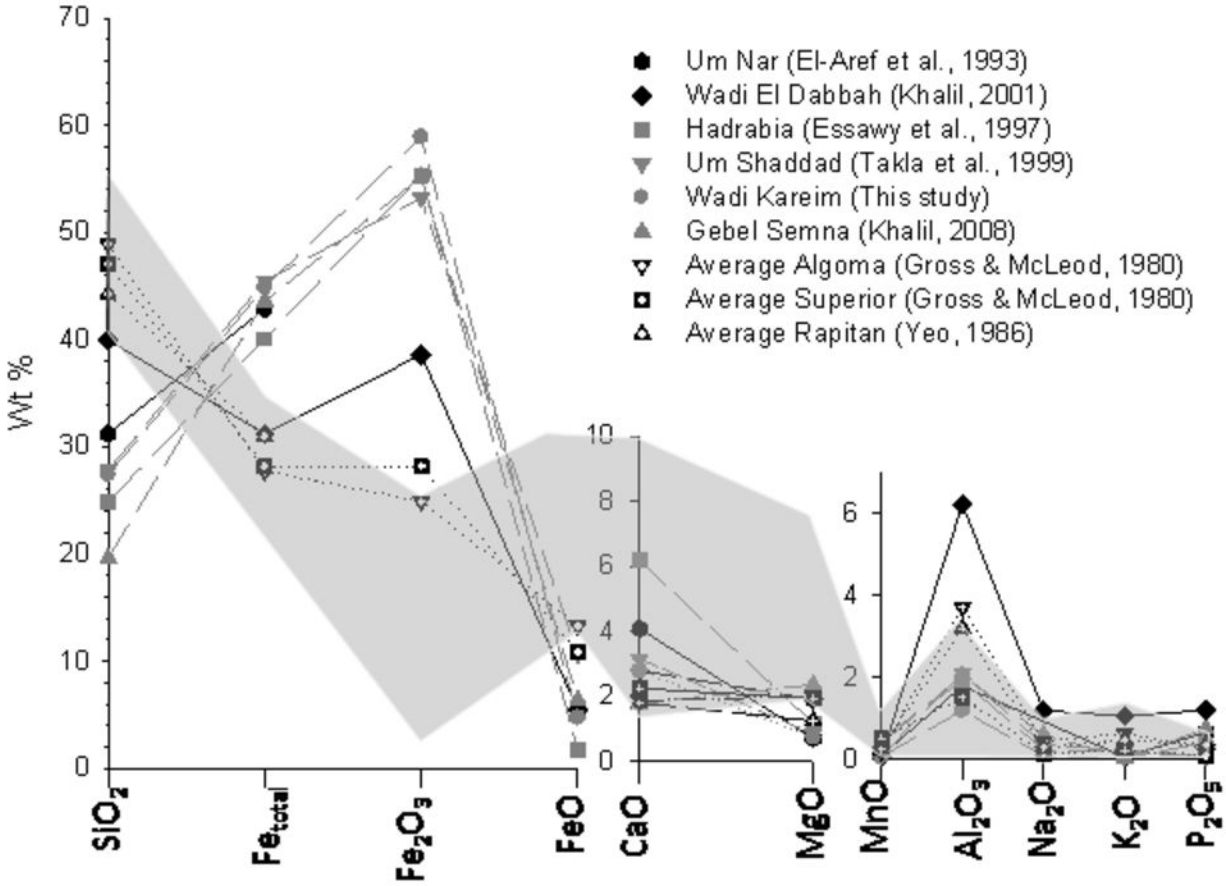
Um Nar (El-Aref et al., 1993)
Wadi El Dabbah (Khalil, 2001)
Hadrabia (Essawy et al., 1997)
Um Shaddad (Takla et al., 1999)
Wadi Kareim (This study)
Gebel Semna (Khalil, 2008)
Average Algoma (Gross & McLeod, 1980)
Average Superior (Gross & McLeod, 1980)
Average Rapitan (Yeo, 1986)
Wt %
70
60
50
40
30
20
10
0
10
8
6
4
2
0
6
4
2
0
SiO_2
Fe_{total}
Fe_2O_3
FeO
CaO
MgO
MnO
Al_2O_3
Na_2O
K_2O
P_2O_5

Fig. 9

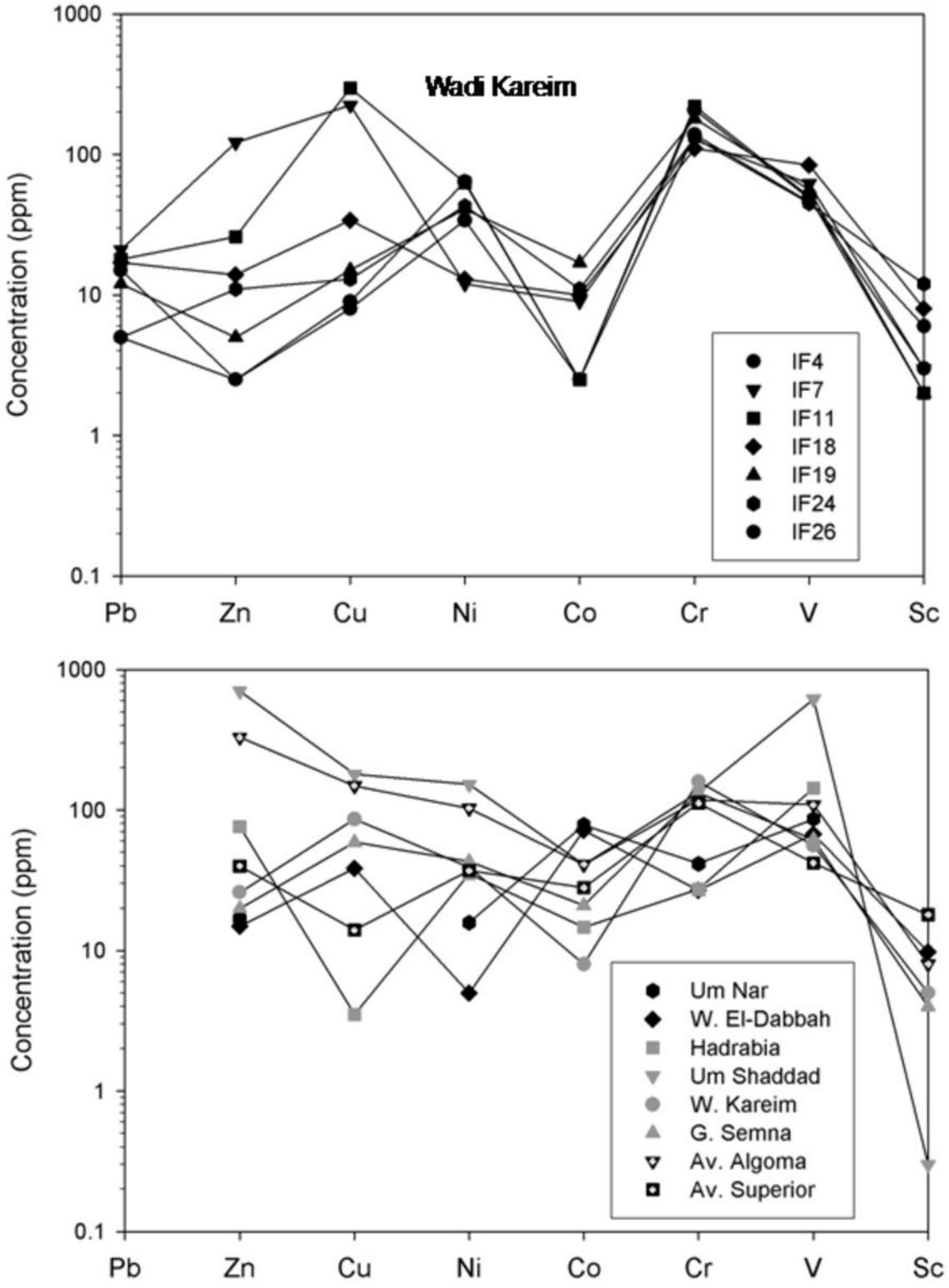
Wadi Kareim
Concentration (ppm)
1000
100
10
1
0.1
Pb
Zn
Cu
Ni
Co
Cr
V
Sc
IF4
IF7
IF11
IF18
IF19
IF24
IF26
Um Nar
W. El-Dabbah
Hadrabia
Um Shaddad
W. Kareim
G. Semna
Av. Algoma
Av. Superior

Fig. 10

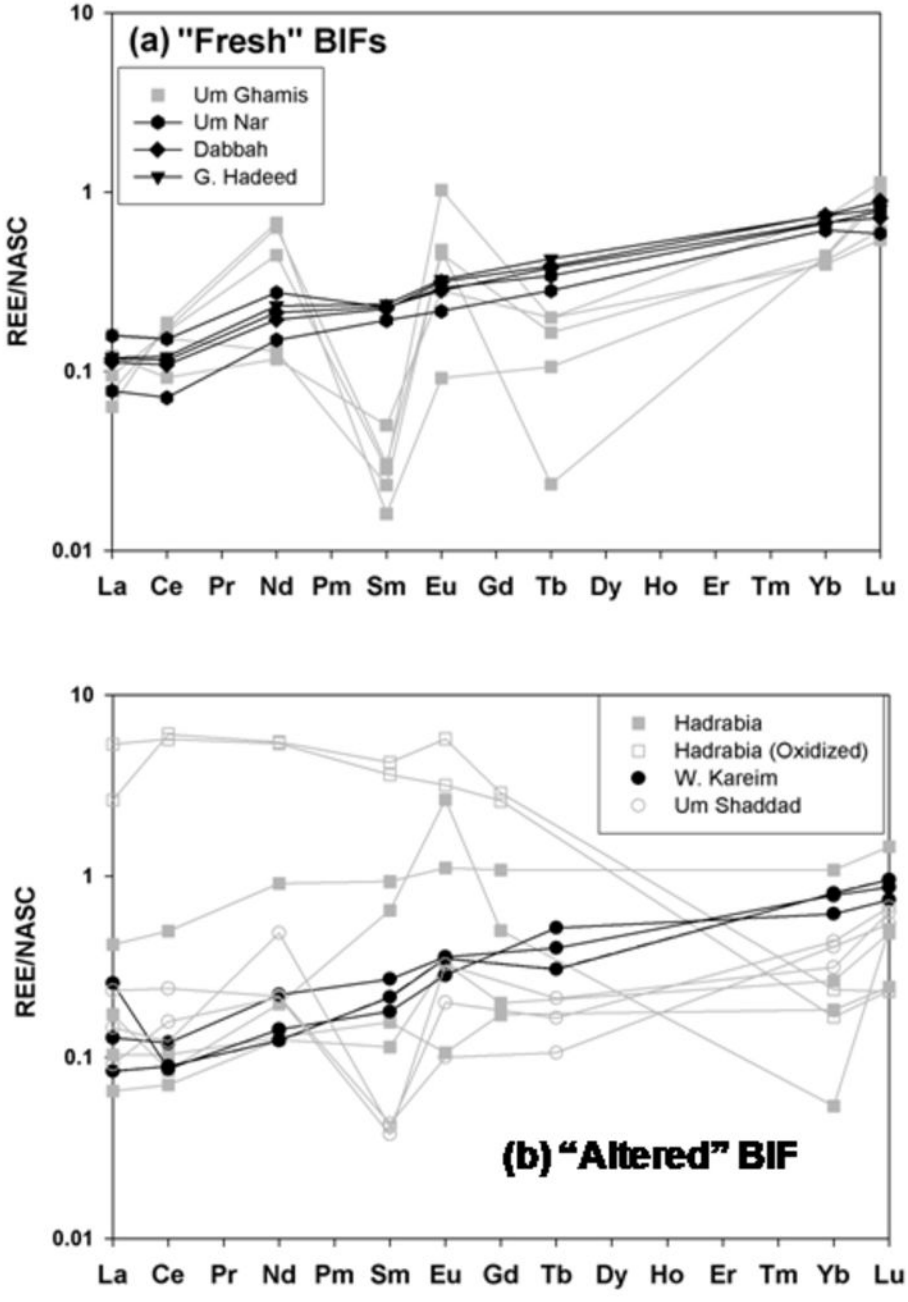
(a) "Fresh" BIFs
Um Ghamis
Um Nar
Dabbah
G. Hadeed
REE/NASC
10
1
0.1
0.01
La Ce Pr Nd Pm Sm Eu Gd Tb Dy Ho Er Tm Yb Lu
Hadrabia
Hadrabia (Oxidized)
W. Kareim
Um Shaddad
(b) "Altered" BIF
REE/NASC
10
1
0.1
0.01
La Ce Pr Nd Pm Sm Eu Gd Tb Dy Ho Er Tm Yb Lu

Fig. 11

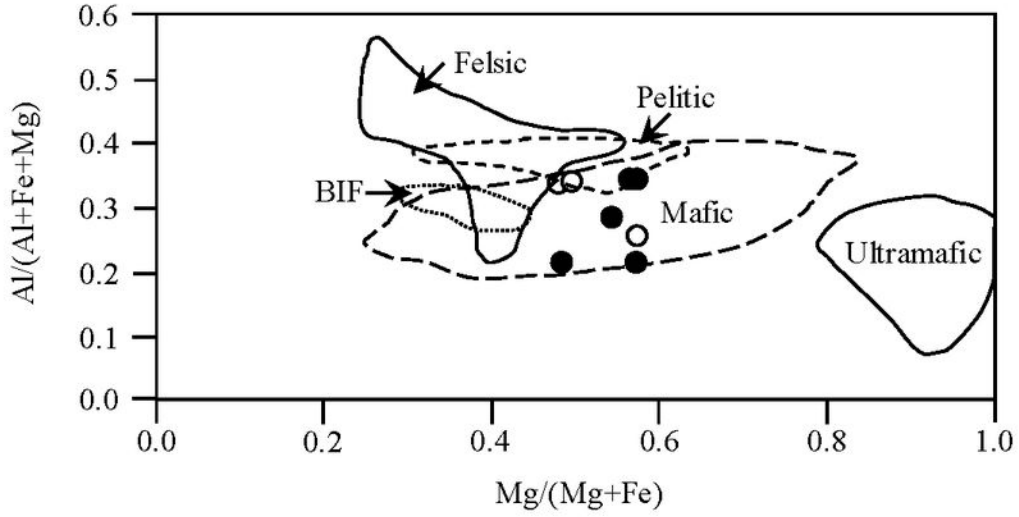
0.6
0.5
0.4
0.3
0.2
0.1
0.0
Al/(Al+Fe+Mg)
0.0
0.2
0.4
0.6
0.8
1.0
Mg/(Mg+Fe)
Felsic
Pelitic
BIF
Mafic
Ultramafic

Fig. 12

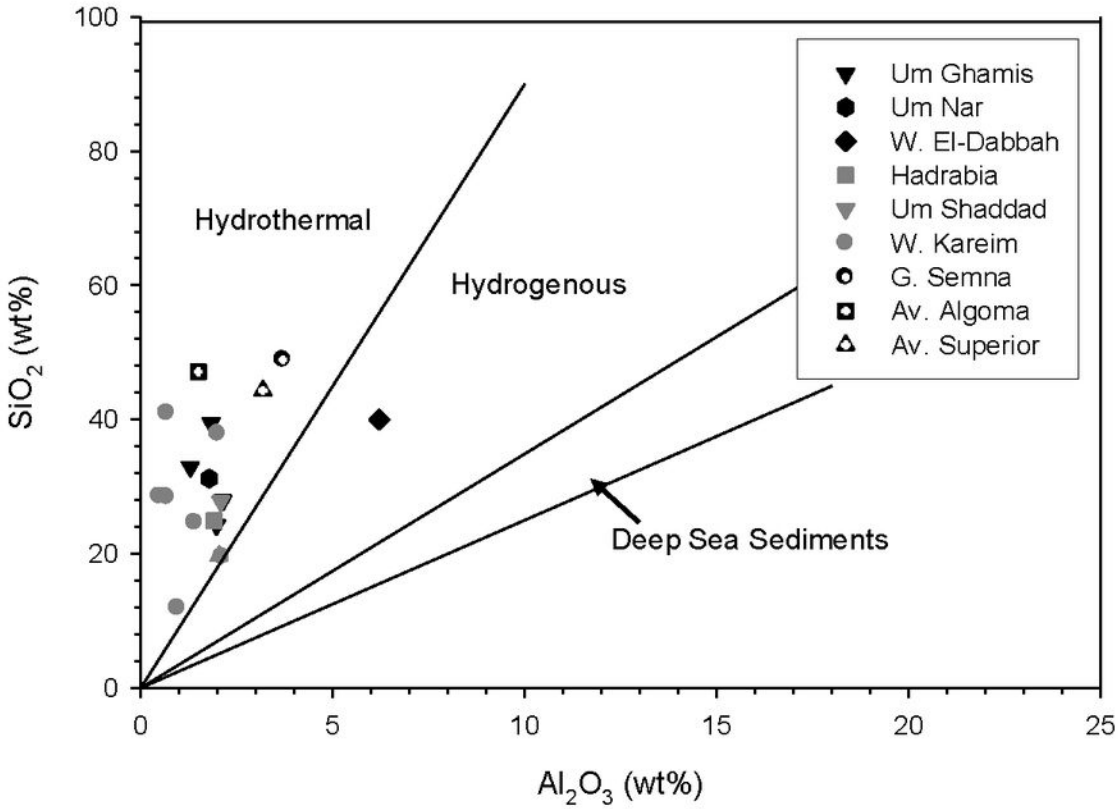
100
80
60
40
20
0
0
5
10
15
20
25
SiO2 (wt%)
Al2O3 (wt%)
Hydrothermal
Hydrogenous
Deep Sea Sediments
Um Ghamis
Um Nar
W. El-Dabbah
Hadrabia
Um Shaddad
W. Kareim
G. Semna
Av. Algoma
Av. Superior

Table 1. *Tectonostratigraphic basement units of the Egyptian Eastern Desert*

Eon/ Era	Tectonic Stage		Age	Rock Types/ Associations		Granitoid intrusion
Phanerozoic	Post-Orogenic		< 570 Ma	Younger Granites (post-tectonic, alkalic): Granite, granodiorite, monzonite.		Gattarian (570–475 Ma)
Neoproterozoic	PanAfrican	Accretion / Collision	600–570	Dokhan metavolcanics (andesite, rhyolite, rhyodacite, pyroclastics) intercalated with Hammamat metasediments (breccias, conglomerates, greywackes, arenites, and siltstones)		
		Subduction	750–650	Island Arc	Shadhli Metavolcanics (rhyolite, dacite, tuff), Volcaniclastic metasediments. Banded Iron Ores	Meatiq (710–610) Hafafit (760–710)
		Spreading	850–750	Ophiolites	Tholeiitic basalt, sheeted dykes, gabbros, serpentinites, all weakly metamorphosed	Shaitian Granite (850–800 Ma)
Archean?/ Paleoproterozoic	Pre-Pan-African		<1.8 Ga	Metasedimentary schists and gneisses (Hb-, Bt-, and Chl- schists), metagreywackes, slates, phyllites, and metaconglomerates		
				Migiff – Hafafit gneiss (Hb and Bt gneiss) and migmatite		

Sources: Egyptian Geological Survey (1981); El-Gaby *et al.* (1990); Hassan and El-Hashad (1990); Stern *et al.* (2006); Avigad *et al.* (2007); Moussa *et al.* (2008).

Table 2. *Representative microprobe analyses of Magnetite and Hematite from Wadi El Dabbah and Wadi Kareim*

	Magnetite													
	W. Dabbah							W. Kareim						
	Host rocks			BIF				Mgt I			Mgt II			
	DH-1	DH-2	DH-3	DBIF-4	DBIF-5	DBIF-6	DBIF-7	K-26-12	K-26-13	K-26-31	K-26-11	K-26-22	K-26-23	K-26-33
SiO_2	1.02	0.74	1.08	0.95	1.18	0.18	0.24	1.69	0.04	1.19	0.04	0.15	0.70	0.85
TiO_2	0.11	0.04	0.15	0.00	0.00	0.00	0.00	0.00	0.00	0.00	0.00	0.00	0.00	0.00
Al_2O_3	0.21	0.12	0.31	0.02	0.04	0.06	0.07	0.00	0.00	0.00	0.00	0.00	0.03	0.03
Cr_2O_3	0.00	0.00	0.00	0.00	0.00	0.00	0.00	0.00	0.00	0.00	0.00	0.00	0.00	0.00
Fe_2O_3	66.44	66.58	66.36	67.42	66.19	68.36	69.21	63.45	68.76	66.51	68.36	68.79	67.22	65.38
FeO	32.17	31.28	32.03	32.50	32.39	31.20	31.71	32.35	30.59	32.36	30.41	31.31	31.76	31.27
MnO	0.00	0.00	0.00	0.00	0.00	0.00	0.00	0.00	0.00	0.00	0.00	0.00	0.00	0.00
MgO	0.20	0.26	0.34	0.00	0.00	0.00	0.00	0.09	0.09	0.23	0.09	0.00	0.10	0.11
CaO	0.12	0.11	0.23	0.09	0.19	0.02	0.04	0.06	0.22	0.00	0.22	0.00	0.00	0.00
NiO	0.00	0.00	0.00	0.00	0.00	0.00	0.00	0.00	0.00	0.00	0.00	0.00	0.00	0.00
ZnO	0.00	0.00	0.00	0.00	0.00	0.00	0.00	0.00	0.00	0.00	0.00	0.00	0.00	0.00
TOTAL	100.27	99.13	100.50	100.98	99.99	99.82	101.26	97.65	99.70	100.29	99.12	100.24	99.82	97.64
Si	0.04	0.03	0.04	0.04	0.05	0.01	0.01	0.07	0.00	0.05	0.00	0.01	0.03	0.03
Ti	0.00	0.00	0.00	0.00	0.00	0.00	0.00	0.00	0.00	0.00	0.00	0.00	0.00	0.00
Al	0.01	0.01	0.01	0.00	0.00	0.00	0.00	0.00	0.00	0.00	0.00	0.00	0.00	0.00
Cr	0.00	0.00	0.00	0.00	0.00	0.00	0.00	0.00	0.00	0.00	0.00	0.00	0.00	0.00
Fe^{+3}	1.91	1.94	1.90	1.93	1.91	1.98	1.98	1.87	2.00	1.91	2.00	1.99	1.94	1.93
Fe^{+2}	1.03	1.01	1.02	1.03	1.04	1.01	1.01	1.06	0.99	1.03	0.99	1.01	1.02	1.03
Mn	0.00	0.00	0.00	0.00	0.00	0.00	0.00	0.00	0.00	0.00	0.00	0.00	0.00	0.00
Mg	0.01	0.01	0.02	0.00	0.00	0.00	0.00	0.01	0.01	0.01	0.01	0.00	0.01	0.01
Ca	0.00	0.00	0.01	0.00	0.01	0.00	0.00	0.00	0.01	0.00	0.01	0.00	0.00	0.00
Ni	0.00	0.00	0.00	0.00	0.00	0.00	0.00	0.00	0.00	0.00	0.00	0.00	0.00	0.00
Zn	0.00	0.00	0.00	0.00	0.00	0.00	0.00	0.00	0.00	0.00	0.00	0.00	0.00	0.00
sum X	1.04	1.02	1.04	1.03	1.04	1.01	1.01	1.07	1.00	1.04	1.00	1.01	1.03	1.04
sum Y	1.92	1.95	1.91	1.93	1.91	1.98	1.98	1.87	2.00	1.91	2.00	1.99	1.94	1.93
Xsp	0.01	0.01	0.02	0.00	0.00	0.00	0.00	0.01	0.01	0.01	0.01	0.00	0.01	0.01
Xga	0.00	0.00	0.00	0.00	0.00	0.00	0.00	0.00	0.00	0.00	0.00	0.00	0.00	0.00
Xusp	0.00	0.00	0.00	0.00	0.00	0.00	0.00	0.00	0.00	0.00	0.00	0.00	0.00	0.00
Xmgt	0.99	0.99	0.99	1.00	1.00	1.00	1.00	1.00	1.00	1.00	1.00	1.00	1.00	1.00
Xhc	0.00	0.00	0.00	0.00	0.00	0.00	0.00	0.00	0.00	0.00	0.00	0.00	0.00	0.00

Table 2. *Representative microprobe analyses of Magnetite and Hematite from Wadi El Dabbah and Wadi Kareim*

	Hematite															
	W. Dabbah					W. Kareim										
	Metasediments				BIF	Metasediments		BIF after Mgt II				BIF after Mgt III				
	Db-8	Db-9	Db-10	Db-11	Db-Sp*	K-35-1	K-35-7	K26-5	K26-21	K26-32	K26-34	K20-4	K20-7	K26-12	K26-13	K26-14
SiO_2	0.93	0.24	0.63	0.95	0.00	1.15	1.07	0.90	0.34	0.32	0.32	2.57	3.35	2.60	1.64	1.19
TiO_2	0.04	0.04	0.04	0.04	0.54	39.36	27.28	0.00	0.00	0.00	0.00	0.00	0.00	0.00	0.00	0.00
Al_2O_3	0.16	0.08	0.32	0.39	0.28	0.53	0.48	0.05	0.00	0.00	0.00	0.19	0.17	0.14	0.04	0.00
Cr_2O_3	0.00	0.00	0.00	0.00	0.00	0.00	0.00	0.00	0.00	0.00	0.00	0.00	0.00	0.00	0.00	0.00
Fe_2O_3	0.00	0.00	0.00	0.00	0.00	0.00	0.00	0.00	0.00	0.00	0.00	0.00	0.00	0.00	0.00	0.00
FeO	88.53	88.24	87.64	88.88	87.20	51.28	62.81	87.96	87.86	87.88	88.39	87.04	86.24	84.93	88.44	88.79
MnO	0.00	0.00	0.00	0.00	0.00	0.00	0.00	0.00	0.00	0.00	0.00	0.00	0.00	0.00	0.00	0.00
MgO	1.01	0.01	0.04	1.19	0.00	0.19	0.11	0.03	0.05	0.08	0.00	0.02	0.02	0.04	0.21	0.12
CaO	0.09	0.14	0.08	0.09	0.06	0.29	0.23	0.00	0.00	0.00	0.00	0.03	0.03	0.80	0.37	0.00
TOTAL	90.76	88.75	88.75	91.54	88.08	92.80	91.98	88.94	88.25	88.28	88.71	89.85	89.81	88.51	90.70	90.10
Si	0.02	0.01	0.02	0.02	0.00	0.03	0.03	0.02	0.01	0.01	0.01	0.07	0.09	0.07	0.04	0.03
Ti	0.00	0.00	0.00	0.00	0.01	0.79	0.55	0.00	0.00	0.00	0.00	0.00	0.00	0.00	0.00	0.00
Al	0.00	0.00	0.01	0.01	0.01	0.02	0.02	0.00	0.00	0.00	0.00	0.01	0.01	0.00	0.00	0.00
Cr	0.00	0.00	0.00	0.00	0.00	0.00	0.00	0.00	0.00	0.00	0.00	0.00	0.00	0.00	0.00	0.00
Fe^{3+}	1.95	1.98	1.95	1.94	1.97	0.34	0.84	1.95	1.98	1.98	1.98	1.86	1.82	1.86	1.91	1.94
Fe^{2+}	0.00	0.00	0.01	0.00	0.01	0.81	0.56	0.02	0.01	0.01	0.01	0.07	0.09	0.05	0.02	0.03
Mn	0.00	0.00	0.00	0.00	0.00	0.00	0.00	0.00	0.00	0.00	0.00	0.00	0.00	0.00	0.00	0.00
Mg	0.04	0.00	0.00	0.05	0.00	0.01	0.00	0.00	0.00	0.00	0.00	0.00	0.00	0.00	0.01	0.00
Ca	0.00	0.00	0.00	0.00	0.00	0.01	0.01	0.00	0.00	0.00	0.00	0.00	0.00	0.02	0.01	0.00
Xhm	0.97	0.99	0.98	0.96	0.99	0.17	0.42	0.98	0.99	0.99	0.99	0.93	0.91	0.93	0.96	0.97
Xilm	0.00	0.00	0.01	0.00	0.01	0.80	0.55	0.01	0.01	0.01	0.01	0.03	0.04	0.03	0.01	0.02

sp: spinel; ga: gahnite; usp: ulvospinel; mgt: magnetite; hc: hercynite; hm: hematite; ilm: ilmenite; * average of four analyses of platy specularite

Table 3. *Representative amphibole analyses from Wadi El-Dabbah BIF*

	139-3 Mg-Hb	129-2 Mg-Hb	129-3 Mg-Hb	129-4 Mg-Hb	129-5 Act-Hb
SiO_2	46.70	47.58	46.19	44.61	50.19
TiO_2	0.32	0.20	0.32	0.93	0.06
Al_2O_3	6.60	6.14	6.99	9.85	3.21
Cr_2O_3	0.00	0.00	0.00	0.00	0.00
FeO	17.34	19.40	18.84	18.08	17.84
MnO	0.80	0.97	0.86	0.83	0.99
MgO	11.38	10.29	10.46	9.70	11.21
CaO	12.30	12.25	12.59	12.20	12.42
Na_2O	0.69	0.66	0.74	1.07	0.37
K_2O	0.31	0.27	0.39	0.47	0.14
Total	96.44	97.76	97.38	97.74	96.43
Si	6.989	7.081	6.922	6.650	7.544
Al^{iv}	1.011	0.919	1.078	1.350	0.456
Al^{vi}	0.154	0.159	0.157	0.382	0.113
Cr	0.000	0.000	0.000	0.000	0.000
Fe^{3+}	0.581	0.567	0.516	0.464	0.194
Ti	0.036	0.022	0.036	0.104	0.007
Mg	2.538	2.282	2.336	2.155	2.511
Fe^{2+}	1.590	1.847	1.846	1.791	2.049
Mn	0.101	0.122	0.109	0.105	0.126
Sum M1-M3	5.000	4.999	5.000	5.001	5.000
Ca^{M4}	1.972	1.953	2.000	1.949	2.000
Na^{M4}	0.028	0.047	0.000	0.051	0.000
Sum M4	2.000	2.000	2.000	2.000	2.000
Ca^{A}	0.000	0.000	0.022	0.000	0.000
Na^{A}	0.173	0.144	0.215	0.258	0.108

Table 3. *Representative amphibole analyses from Wadi El-Dabbah BIF*

K^A	0.059	0.051	0.075	0.089	0.027
Sum A	0.232	0.195	0.311	0.347	0.135
X_{Mg}	0.615	0.553	0.559	0.546	0.551
Al^T	1.165	1.078	1.235	1.732	0.569

Table 4. *Average and representative microprobe analyses of chlorite and stilpnomelane from selected the Egyptian BIFs*

	Chlorite								Stilpnomelane		
	W. El Dabbah Khalil, 2001			W. Kareim metasediments				G. Semna Khalil, 2008		W. Kareim	
				35/3	35/14	35/15	35/21	av. n=3		anhedral av. n=3	fibrous av. n=3
SiO_2	31.257	27.472	28.599	27.020	26.840	27.340	29.390	27.43	SiO_2	43.58	32.98
TiO_2	0.000	0.238	0.331	0.000	0.000	0.000	0.000	0.08	CaO	2.16	0.69
MnO	0.093	0.228	0.786	0.300	0.330	0.340	0.300	0.13	K_2O	1.25	2.95
FeO	28.351	28.103	22.724	12.380	13.440	12.930	13.100	26.68	Na_2O	0.22	0.49
MgO	14.905	20.614	16.229	22.700	23.200	22.250	22.740	16.45	FeO	36.97	35.16
Al_2O_3	10.602	12.588	19.207	24.180	24.700	24.090	23.420	17.08	MgO	1.79	5.32
$H_2O_{calc.}$	12.888	11.540	11.730	12.040	11.430	11.190	11.160	11.44	Al_2O_3	8.67	15.73
Total	98.10	100.78	99.61	98.62	99.94	98.14	100.11	99.29	$H_2O_{calc.}$	5.62	5.71
									Total	100.26	99.00
Structural formula based on 10 cations									Structural formula based on 7 cations		
Si	3.482	2.835	2.999	2.688	2.615	2.683	2.877	2.901	Na	0.035	0.075
Al^{IV}	0.518	1.165	1.001	1.312	1.385	1.317	1.123	1.099	Ca	0.185	0.058
Total	4.000	4.000	4.000	4.000	4.000	4.000	4.000	4.000	K	0.127	0.296
Al^{VI}	0.874	0.366	1.374	1.524	1.450	1.471	1.579	1.03	Total	0.347	0.429
Ti	0.000	0.018	0.026	0.000	0.000	0.000	0.000	0.01	Al	0.312	0.058
Mn	0.009	0.020	0.070	0.025	0.028	0.029	0.031	0.012	Fe	2.475	2.316
Fe^{+2}	2.642	2.425	1.993	1.030	1.094	1.062	1.073	2.360	Mg	0.213	0.626
Mg	2.475	3.171	2.537	3.367	3.428	3.256	3.317	2.592	Total	3.000	3.000
Total	6.000	6.000	6.000	6.000	6.000	6.000	6.000	*6.000*	Si	3.494	2.598
									Al	0.506	1.402
Fe/(Fe+Mg)	0.516	0.433	0.440	0.234	0.242	0.246	0.244	0.477	Total	4.000	4.000

Table 5. *Representative garnet analyses from W. Kareim and W. El-Dabbah*

	W. Kareim Metasediments					W. El-Dabbah BIF				Metasediemnts		
	35/11	35/33	35/22	35/12	35/21	129/6	116/7	127/14	127/18	133/2	133/5	129/5
SiO_2	38.60	37.84	38.27	38.82	38.10	37.90	37.64	38.31	37.74	38.45	37.69	37.40
TiO_2	0.26	0.22	0.18	0.13	0.13	0.28	0.09	0.08	0.05	0.34	0.07	0.24
Al_2O_3	21.99	21.37	21.31	21.71	21.09	21.29	21.20	21.36	21.43	21.58	21.36	21.48
Fe_2O_3	1.32	0.43	0.73	0.50	0.96	0.56	0.59	0.34	0.39	0.51	0.41	0.79
V2O3	0.00	0.00	0.00	0.00	0.03	0.00	0.20	0.04	0.03	0.04	0.05	0.03
FeO	15.31	14.92	14.09	14.63	13.99	15.38	14.82	15.04	15.62	16.05	16.56	14.89
MnO	0.20	0.21	0.52	0.09	0.04	0.48	0.31	0.07	0.03	0.21	0.20	0.46
MgO	0.23	0.00	0.00	0.00	0.00	0.20	0.20	0.51	0.03	0.00	0.00	0.05
CaO	23.79	24.13	24.62	24.90	25.01	23.34	24.39	23.73	24.08	23.58	23.15	23.91
Total	100.91	99.12	99.72	100.78	99.30	99.33	99.44	99.48	99.40	100.76	99.49	99.25
Structural formula based on 8 cations												
Si	2.981	2.967	2.982	2.989	2.979	2.969	2.941	2.977	2.952	2.974	2.954	2.948
Ti	0.016	0.014	0.011	0.008	0.008	0.016	0.005	0.005	0.003	0.020	0.004	0.014
Total	2.997	2.931	2.993	2.997	2.987	2.985	2.946	2.982	2.955	2.994	2.958	2.962
Al	1.929	1.975	1.957	1.971	1.942	1.967	1.952	1.956	1.975	1.968	1.973	1.951
Fe^{3+}	0.071	0.025	0.043	0.029	0.056	0.033	0.035	0.020	0.023	0.030	0.024	0.047
V	0.000	0.000	0.000	0.000	0.002	0.000	0.013	0.024	0.002	0.002	0.003	0.002
Total	2.000	2.000	2.000	2.000	2.000	2.000	2.000	2.000	2.000	2.000	2.000	2.000
Fe^{2+}	0.995	0.978	0.918	0.942	0.915	1.008	0.968	0.978	1.022	1.038	1.085	0.981
Ca	1.968	2.027	2.055	2.055	2.095	1.951	2.042	1.976	2.017	1.954	1.944	2.020
Mn	0.013	0.014	0.034	0.006	0.003	0.032	0.020	0.005	0.002	0.014	0.013	0.031
Mg	0.027	0.000	0.000	0.000	0.000	0.024	0.024	0.059	0.004	0.000	0.000	0.006
Total	3.003	3.019	3.003	3.003	3.013	3.015	3.054	3.018	3.045	3.045	3.042	3.038
Alamandine %	33.17	32.39	30.53	31.40	30.37	33.43	31.70	32.40	33.56	34.52	35.67	32.70
Pyrope %	0.90	0.00	0.00	0.00	0.00	0.80	0.80	1.96	0.13	0.00	0.00	0.20
Grossularite %	61.97	65.87	66.17	66.93	66.60	63.07	64.39	63.23	64.99	63.37	62.55	63.60
Spessartite %	0.43	0.47	1.13	0.20	0.10	1.07	0.67	0.17	0.07	0.47	0.43	1.03
Andradite %	3.00	0.80	1.80	1.20	2.56	1.10	1.60	0.87	1.05	0.87	1.05	1.90
Schorlomite %	0.53	0.47	0.37	0.27	0.27	0.53	0.17	0.17	0.10	0.67	0.13	0.47
Goldmanite	0.00	0.00	0.00	0.00	0.10	0.00	0.67	1.20	0.10	0.10	0.17	0.10

Table 6. *Representative analyses of carbonates from Wadi Kareim Wadi El GDabbah*

	Wadi Kareim Metasediments early			late			BIF early		late					Wadi El-Dabbah Metasediments		BIF
	36/6	35/8	35/15	35/1	35/9	35/10	26/10	26/0	1-Apr	26/1	26/8	26/11	26/14	108/9	108/11	108/36
CaO	51.85	59.25	54.76	62.16	60.55	58.35	36.13	32.55	57.54	53.82	57.01	59.15	59.49	58.34	58.86	59.79
FeO	0.83	0.37	0.23	0.00	0.05	0.08	19.35	23.48	2.31	0.92	1.53	1.98	1.46	1.15	0.70	1.08
MnO	0.11	0.53	0.50	0.00	0.00	0.00	0.63	0.51	0.35	0.39	0.51	0.32	0.80	0.48	0.54	0.09
MgO	0.61	0.24	0.19	0.00	0.03	0.04	1.43	1.97	0.63	0.44	0.24	0.38	0.21	0.30	0.27	0.07
CO_2*	46.19	40.94	44.39	39.70	40.71	42.21	42.15	42.39	38.92	44.50	41.87	38.29	38.39	41.11	40.98	40.59
Total	99.59	101.33	100.67	101.86	101.26	100.68	99.69	100.90	99.75	100.07	101.16	100.12	100.35	101.38	101.35	101.62
Mole % end member																
Calcite	94.00	96.60	97.00	100.00	99.80	99.60	63.60	55.20	90.20	94.00	93.40	92.40	93.80	94.40	95.60	96.60
Siderite	2.40	1.00	0.60	0.00	0.20	0.22	28.10	33.90	6.00	2.60	4.00	5.00	3.60	3.00	1.80	2.80
Dolomite	3.20	1.00	1.00	0.00	0.20	0.18	7.40	10.20	2.80	2.20	1.20	1.80	1.00	1.40	1.20	0.40
Rhodochrosite	0.40	1.40	1.40	0.00	0.00	0.00	0.90	0.70	1.00	1.20	1.40	0.80	1.60	1.20	1.40	0.20

CO_2* is calculated according to the formulae.

Table 6. *Representative analyses of carbonates from Wadi Kareim Wadi El GDabbah*

108/6
50.76
4.05
0.30
0.27
45.26
100.64
86.20
11.60
1.40
0.80

Table 7. *Whole rock chemical compositions of Wadi Kareim samples*

	V1	V2	V3	Av.	S.D.	S2	S3	S28	S1	S2	S27	Av.	S.D.	IF4	IF7	IF11	IF18	IF19	IF24	IF26	Av.	S.D.
SiO_2	56.01	58.62	58.21	57.61	1.40	68.70	67.10	61.10	63.05	60.99	59.00	63.32	3.80	28.56	11.92	28.46	19.52	24.62	40.96	37.88	27.42	10.05
TiO_2	0.97	0.68	0.79	0.81	0.15	0.58	0.61	0.71	0.62	0.73	0.91	0.96	0.12	0.06	0.08	0.07	0.18	0.09	0.06	0.12	0.09	0.04
Al_2O_3	15.59	14.11	14.63	14.78	0.75	11.50	12.50	12.90	11.71	13.53	11.60	12.29	0.82	0.48	0.95	0.67	2.11	1.40	0.67	2.00	1.18	0.66
Fe_2O_3	6.20	5.77	4.86	5.61	0.68	2.64	1.73	1.95	1.48	1.87	1.47	1.86	0.43	60.67	78.94	63.37	63.08	62.50	35.67	48.13	58.91	13.61
FeO	3.36	3.01	3.57	3.31	0.28	4.08	4.49	5.58	6.01	5.26	6.07	5.25	0.81	3.80	5.52	2.57	6.70	8.28	1.09	5.16	4.73	2.45
MnO	0.14	0.24	0.23	0.20	0.06	0.06	0.09	0.13	0.31	0.25	0.13	0.16	0.10	0.04	0.05	0.03	0.05	0.02	0.11	0.04	0.05	0.03
MgO	4.37	3.95	4.13	4.15	0.21	2.16	2.43	4.46	3.69	3.25	4.82	3.47	1.07	0.40	0.80	0.33	1.83	0.81	0.45	0.58	0.74	0.51
CaO	4.61	6.11	5.89	5.54	0.81	2.07	3.11	5.03	4.78	6.11	5.90	4.50	1.60	2.87	0.63	0.45	2.57	1.48	9.31	2.13	2.78	3.02
Na_2O	3.01	2.69	2.98	2.89	0.18	1.64	2.64	2.43	3.31	2.91	2.46	2.57	0.56	0.05	0.09	0.04	0.07	0.05	0.09	0.10	0.07	0.02
K_2O	0.53	0.71	0.92	0.72	0.20	1.37	1.84	0.20	0.68	0.52	2.84	1.24	0.98	0.03	0.04	0.02	0.02	0.01	0.03	0.02	0.02	0.01
P_2O_5	0.20	0.23	0.13	0.19	0.05	0.13	0.17	0.13	0.22	0.19	0.14	0.16	0.04	0.31	0.21	0.50	0.74	0.39	0.13	0.42	0.39	0.20
H_2O^-	0.23	0.21	0.28	1.04	0.04	0.51	0.50	0.73	0.62	0.68	0.69	0.68	0.10	0.29	0.60	0.45	0.29	0.27	0.57	0.08	0.36	0.19
L.O.I.	3.59	2.79	2.34	2.91	0.63	3.90	2.55	5.22	3.01	3.81	3.10	3.60	0.94	2.50	1.78	1.97	2.34	0.42	9.06	1.44	2.79	2.85
Total	98.99	99.14	98.89	99.01	0.13	99.87	99.77	100.34	99.60	100.04	99.13	99.79	0.41	100.10	101.61	98.93	99.50	100.34	98.20	98.10	99.53	1.26
$Fe_2O_3^T$	9.93	9.12	8.83	9.29	0.57	7.17	6.72	8.15	8.16	7.72	8.21	7.69	0.62	64.89	85.07	66.23	70.53	71.70	36.88	53.86	64.17	15.22
Fe^T	6.95	6.38	6.18	6.50	0.40	5.01	4.70	5.70	5.71	5.40	5.74	5.38	0.43	45.39	59.50	46.32	49.33	50.15	25.79	37.67	44.88	10.65
Si	26.17	27.39	27.20	26.92	0.66	32.10	31.35	28.55	29.46	28.49	27.56	29.58	1.78	13.34	5.57	13.30	9.12	11.50	19.14	17.70	12.81	4.69
Nb	7	7	10	8	2	5	7	6	5	5	7	6	1	3	3	2	3	2	7	2	3	2
Zr	50	85	54	63	19	93	101	126	91	125	113	108	15	16	15	19	36	20	23	13	20	8
Y	31	24	21	25	5	16	19	25	14	21	29	21	6	20	11	22	11	26	14	20	18	6
Sr	213	191	184	196	15	106	166	142	161	148	180	151	26	43	34	83	86	54	73	103	68	25
Rb	10	16	15	14	3	31	24	2.5	21	16	42	23	13	3	3	2	4	2	2	3	3	1
Pb	41	50	95	62	29	5	5	5	5	5	5	5	0	15	21	18	17	12	5	5	13	6
Ga	14	14	19	16	3	12	11	13	10	9	13	11	2	2	3	3	4	2	2	3	3	1
Zn	115	79	83	92	20	61	49	67	66	62	58	61	7	2.5	122	26	14	5	11	2.5	26	43
Cu	74	91	97	87	12	31	25	31	32	22	19	27	5	8	224	298	34	15	13	9	86	122
Ni	45	39	51	45	6	34	45	41	29	39	25	36	8	34	12	63	13	41	43	64	39	21
Co	92	87	124	101	20	14	11	17	231	18	22	52	88	2.5	9	2.5	10	17	11	2.5	8	6
Cr	95	110	76	94	17	51	39	46	41	51	58	48	7	139	127	220	110	180	132	207	159	43
V	225	240	231	232	8	98	146	134	125	111	108	120	18	46	62	50	84	56	45	49	56	14
Ba	91	65	59	72	17	220	107	38	45	68	308	131	109	37	31	44	28	30	54	33	37	9
Sc	20	19	22	20	2	12	17	19	21	26	15	18	5	6	3	2	8	2	12	3	5	4

Av. Average; S.D.: standard deviation. Major element concentrations in weight %, trace elements in ppm.

Table 8. *Average major (wt %) and trace (ppm) element compositions of some* Egyptian BIFs compared to average Algoma, Lake Superior and Rapitan types

	"Fresh" BIF			"Altered" BIF					
	Um Shadad	Um Nar	W. El Dabbah	Hadrabia BIF	W. Kareim	G. Semna	Algoma BIF	Superior BIF	Rapitan BIF
	Takla *et al.* , 19	EL Aref *et al.* , 19	Khalil, 2001	Essawy *et. al., 1997*		Khalil, 2008	Gross & McLeod, 1980		Yeo, 1986
SiO_2	27.81	31.19	39.96	24.87	27.42	19.64	48.90	47.10	44.30
TiO_2	0.08	0.12	0.31	0.09	0.09	0.63	0.12	0.04	0.27
Al_2O_3	2.08	1.78	6.21	1.90	1.18	2.04	3.70	1.50	3.18
Fe_2O_3	53.20	n.r.	38.60	55.33	58.91	55.17	24.90	28.20	n.r
FeO	10.66	n.r.	5.42	1.75	4.73	6.40	13.30	10.90	n.r.
MnO	0.07	0.08	0.06	0.50	0.05	0.37	0.19	0.49	0.23
MgO	0.83	0.71	1.89	1.16	0.74	2.35	2.00	1.93	1.24
CaO	3.15	4.08	2.79	6.18	2.78	1.76	1.87	2.24	1.79
Na_2O	0.34	n.r.	1.18	0.21	0.07	0.58	0.43	0.13	0.28
K_2O	0.20	0.04	1.05	0.16	0.02	0.02	0.62	0.20	0.45
P_2O_5	0.06	0.65	1.19	0.05	0.39	0.73	0.23	0.08	0.35
$Fe_2O_3^T$	65.05	61.29	44.62	57.27	64.17	62.29	39.68	40.31	44.30
Fe^T	45.5	42.9	31.2	40.1	44.9	43.6	27.8	28.2	31.0
Si	13.0	14.6	18.7	11.6	12.8	9.2	22.8	22.0	20.7
Zr	43	47.60	77	73	20	21	98	81	n.r.
Y	45	46.53	36	20	18	26	54	47	n.r.
Sr	70	87.35	77	89	68	61	116	37	n.r.
Zn	701	16.98	15	76	26	20	330	40	n.r.
Cu	180	n.r.	39	4	86	59	149	14	n.r.
Ni	152	15.81	5	35	39	43	103	37	n.r.
Co	41	78.33	72	15	8	21	41	28	n.r.
Cr	134	41.60	27	27	159	133	118	112	n.r.
V	617	86.35	67	144	56	62	109	42	n.r.
Sc	0.30	n.r.	10	n.r.	5	4	8	18	n.r.

n.r. = not reported

$Fe_2O_3^T$ = Total iron as Fe_2O_3

Table 9. *Characteristics of the Egyptian BIFs in comparison with Algoma, Superior, and Rapitan types*

	Algoma	Superior	Rapitan	Egyptian BIF	
				"Fresh"	"Altered"
Age (Ga)	> 2.5	2.5–1.9	0.8–0.6	0.85?–0.65	0.75–0.6
Size	small	large	small	small	small
Thickness	< 50 m	> 100 m	75–270 m	v. thin	5–30 m
Deformation	V. strong	Undeformed	Deformed	Strong	Strong
Facies	O, Si, Sf ± C	O, Si, C	O, Si, ± C	O, Si, ± C	O, Si, ± C
Oolites	rare	always	common	none	none
Ore Minerals	Mgt>Hm	Mgt > Hm higher Hm	Hm	Mgt > Hm	Mgt ≥ Hm
Rock Associations	Thol to CA vol., tuffs, wackes/ shales	Carbonaceous shales	Diamictites	CA volcanic, tuffs, shales wackes; diamictites?	
Chemistry	High Cr, Mn, Ni, Cu, As	Low Cr, Co, Ni, Cu, Zn.	High P, Fe, low Cr, Co, Ni	Low Cr, Co, Ni, Cu variable Al	
REE/NASC	+ Eu, - Ce, slight HREE-enrichment	+ Eu, Strong HREE-enrichment	Weak + Eu v. strong HREE enrichment	- Sm, + Nd & Eu HREE - enriched	+Eu, -Yb LREE-rich
Fe/Si	< 1.36	< 1.36	1.3–1.6	1.4–2.75	3–4.7
Fe_2O_3/FeO	1.9	2.76	46–100	5.5–8	7–57

O = oxide, Si = silicate, C = carbonate, Sf = sulfide, Mgt = magnetite, Hm = hematite.